Article:

Kneller, B, Bozetti, G, Callow, R et al. (8 more authors) (2020) Architecture, process, and environmental diversity in a late Cretaceous slope channel system. Journal of Sedimentary Research, 90 (1). pp. 1-26. ISSN 1527-1404

https://doi.org/10.2110/jsr.2020.1

ARCHITECTURE, PROCESS AND ENVIRONMENTAL DIVERSITY IN A LATE CRETACEOUS SLOPE CHANNEL SYSTEM

Benjamin Kneller[1*], Guilherme Bozetti[1,9], Richard Callow[1,2], Mason Dykstra[3], Larissa Hansen[1,6], Ian Kane[2,4], Pan Li[1, 8]†, Adam McArthur[5,6], Amanda Santa Catharina[1], Thisiane dos Santos[1] and Philip Thompson[1,7]

1. School of Geosciences, University of Aberdeen, Aberdeen AB24 3UE, UK (*corresponding author)

2. Equinor ASA, 4035 Stavanger, Norway

3. Anadarko Petroleum Corporation, 1201 Lake Robbins Drive, The Woodlands, Texas 77380, USA

4. School of Earth and Environmental Sciences, The University of Manchester, Oxford Rd, Manchester, M13 9PL, UK

5. Universidade Federal do Rio Grande do Sul, Avenida Paulo Gama, 110, Bairro Farroupilha, Porto Alegre, Rio Grande do Sul, Brazil

6. School of Earth and Environment, University of Leeds, Leeds, LS2 9JT, UK

7. Shell International Ltd., 40 Bank Street, Canary Wharf, London, E14 5NR

8. Research Institute of Petroleum Exploration and Development, PetroChina, Beijing, 100083, China (†Chinese correspondence to be addressed to lipanccc@126.com)

9. Department of Ocean Sciences and Engineering, Southern University of Science and Technology, 1088 Xueyuan Road., Shenzhen, 518055, China

ABSTRACT

Arroyo San Fernando on the Pacific coast of Baja California, Mexico, provides a superb view of the architecture of a Maastrichtian active margin slope channel system and the record of its evolution through a third-order sea-level cycle. The succession is organized into architectural building blocks (channel complex sets) consisting of a channel belt with an axial region and a channel belt margin of terraces and internal levees. The channel belt is confined by an external levee on one side and by an erosion surface into the slope on the other. Each channel complex set can be subdivided into three stages of evolution: Stage I consists of highly amalgamated coarse-grained channel complexes; Stage II consists of gravelly meander belts with marginal and stratigraphically intervening thin-bedded turbidites; and Stage III consists of mudstones representing abandonment. This succession is associated with repeated and therefore predictable changes in architecture, facies distribution, inferred seafloor morphology and sedimentary process. We describe variability in the sedimentology, ichnology, palynology, provenance and inferred sedimentary processes between and within these architectural elements. Channel formation and fill are attributed to erosion, sediment transport and deposition by turbidity currents and lesser debris flows. Ichnology indicates enhanced oxygenation and supply of organic material, substrate type and turbidity within the channel belt; the axial region may be differentiated from the terraces by differing response to turbidity current intensity. Levee environments show ichnological gradients away from the channel towards background slope. Palynology reflects confinement of the supply of terrigenous material to the channel belt but is also indicative of stratification within the turbidity currents, as is the distribution of heavy minerals. Provenance is from the extinct portion of the continental margin arc to the east, via high-gradient gravelly streams

and across a steep shoreline, with direct supply of coastal material to deep water. Architectural hierarchy bears comparison with other slope channel systems, but in common with them the fill represents only a small fraction of the time that the system was active.

INTRODUCTION

Slope channels on basin margins represent pathways through which sediment is delivered to depositional sites lower on the slope or on the basin floor. Slope channels commonly have erosional basal bounding surfaces, and/or are flanked by levees (e.g. Kolla and Coumes 1987; Deptuck et al. 2003). These erosional surfaces commonly represent periods of time when bypass of sediment was complete (Hodgson et al. 2006; Stevenson et al. 2013, 2015; Hodgson et al. 2016; Hansen et al. 2017b), when all of the sediment, moved by whatever sediment transport processes were operating within the channel, was carried further down-dip. Given the constraints we describe below, this might represent 1000´s of km^3 of sediment.

Sediment accumulating within the channel (i.e. the ‘channel fill’) represents episodes when the down-dip transport of sediment was not complete, and the channel was operating at less than 100% efficiency as a sediment conduit. Typically, channel fills do not consist of a monotonic continuous succession but show alternations between the two states of erosion and deposition (e.g. Kneller 2003), with deposition tending to become increasingly dominant as the channel fill evolves (e.g. McHargue et al. 2011). One consequence of this is that the form of a channel fill as preserved in the geological record typically bears a complicated relationship, if any, with the form of the parent channel as it existed on the sea floor (Gamberi et al. 2013 and references therein). Nonetheless, the general style of channel may be reconstructed by the recognition of various depositional elements within the channel fills, at least in a gross sense.

This study describes the fill of an ancient coarse-grained slope channel system, by which we mean the composite fill of a succession of channels at approximately the same position on the sea floor over a significant period of time (perhaps ~1.6 Myr, Dykstra and Kneller 2007), which successively filled the same erosional/levee-bounded conduit, albeit with modification of the bounding surfaces over time. We describe the gross architecture, and the distribution of depositional elements identified through their sedimentology, lithofacies associations, geometry, and elements of their sediment provenance, ichnology and palynofacies, to create an integrated interpretation of the system. While we do not suggest that this is a universal model for coarse-grained slope channel systems, it does bear notable comparison in scale and architecture with some more recent slope channel systems (e.g. Depuck et al. 2003; Nakajima et al. 2009), and also with some published models for ancient slope channel systems that have been used as a basis for hydrocarbon reservoir models (e.g. Mayall and and Stewart 2000; Sprague et al. 2002; McHargue et al. 2011). It also allows us to make some inferences about the processes that occur within these systems.

GEOLOGICAL SETTING

The Late Cretaceous age rocks described here form part of the Rosario Formation (Morris and Busby-Spera 1990; see below), deposited on an active continental margin that constituted the Peninsular Ranges fore-arc (Busby et al. 1998), roughly parallel to the course of the present Mexican coastline. This faced the paleo-Pacific Ocean (Gastil et al. 1974; Morris and Busby-Spera 1990; Morris 1992) and was possibly confined to the west by an actively accreting subduction complex (Dickinson 1985; Williams and Graham 2013). The source of sediment lay in the extinct portion of the arc immediately to the east, yielding zircon provenance ages of around 90-100 Ma (Sharman et al. 2015; see below). The volcanically active part of the arc had by this time migrated eastwards into what is now Sonora in the Mexican mainland (Lipman 1992; McDowell et al. 2001). The contemporaneous coastline to the system described in this study is believed to have lain approximately 20 km to the ENE of the outcrops described here (Busby et al. 2002). The nature of this margin was transformed by the subsequent separation of Baja California from the Mexican mainland by the opening of the Gulf of California commencing at about 6 Ma (Oskin and Stock 2003).

The slope channel system we describe (the San Fernando Channel System; Morris and Busby-Spera 1990) is located on the central west coast of the Baja California peninsula (Fig. 1). The environment is arid and the region is essentially desert, with extremely sparse vegetation except in the larger, alluvium-filled valleys. The land surface consists largely of a low-gradient gravel-covered pediment defining a paleo-land surface, locally overlying a weathering profile of probable late Neogene age. This surface is dissected by erosion of presumed Pleistocene age, generating extensive fresh exposures on the steeper valley sides but with rather poorer exposure on the gentler slopes. The rocks are poorly cemented and have experienced little burial, spore colour index indicating less than 1 km, assuming normal geothermal gradients. Northeasterly tectonic dips in the study area are fairly uniform and rarely more than 5 degrees. There is little post-depositional faulting although parts of the system show syn-sedimentary faulting.

This succession was described by Morris and Busby-Spera (1990) as a submarine fan valley-levee complex. It has also been studied by Dykstra and Kneller

(2007) and Kane et al. (2007) who described it as an asymmetric slope channel system with a well-developed external levee (*sensu* Kane and Hodgson 2011) on one side only, due to its implied structurally-controlled obliquity to the slope (Dykstra and Kneller 2007; Kane et al. 2007).

The system is of upper Maastrichtian age (Dykstra and Kneller 2007), and is immediately and conformably overlain by Paleocene rocks. This study differs slightly from previous accounts in that we consider the lower elements described by Dykstra and Kneller (2007) and Kane et al. (2007, 2009) to belong to an older system (early Maastrichtian). Water depths were bathyal (~1500 to 3000 m) according to benthic foraminiferal assemblages (Dykstra and Kneller 2007).

The work presented here is based on ground mapping, photomosaic interpretation, use of high-resolution satellite imagery, more than 3000 m of sedimentary logging, ichnology, heavy mineral analysis, palynology and grain-size distributions.

STRATIGRAPHIC ORGANIZATION

The slope channel system consists of a circa 380 m thick, 5 to 7 km wide succession of conglomerates, sandstones, siltstones and mudstones, bounded to the north-west by a roughly 3 km wide belt of very regularly inter-bedded sandstones and mudstones, interpreted by Morris and Busby-Spera (1990), Dykstra and Kneller (2007) and Kane et al. (2007) as an external levee. The majority of the conglomerates lie within a belt (which we refer to as the *axial region,* fringed by a loosely defined *off-axis*), up to approximately 5 km wide. This is separated from the external levee to the NW by a 1 to 3 km wide zone of dominantly thin-bedded sandstones and mudstones, which we refer to as *channel belt margin*. Together we refer to the axial and marginal regions as the *channel belt*. To the south-east the axial region onlaps pale, slightly calcareous mudstones, interpreted as background, dominantly hemipelagic slope sediments (Fig. 2; Dykstra and Kneller 2007; Kane et al. 2007). Paleocurrents deduced from *a*-axis imbrication of gravels in conglomerates and ripple cross-lamination in sandstones of the channel belt are dominantly towards the south-south-west (Fig. 2; Morris and Busby-Spera 1990; Dykstra and Kneller 2007).

Channel Complex Set Architecture

Facies.---

The conglomerates form part of distinct packages ranging from 50 to 140 m thick. Each package generally consists of two or three distinct intervals. A lower interval (Stage I) consists of amalgamated conglomerates and very subordinate sandstones, and is internally made up of smaller, amalgamated, erosionally-based packages called *channel complexes* (that are often difficult to differentiate within Stage I), and bounded below by a distinct and laterally traceable erosion surface (Figs 2, 3, 4) (cf Fildani et al. 2013). An upper interval (Stage II) contains discrete units of conglomerate, of the order of 10 m thick and hundreds of meters wide, and each bounded below by a shallow erosion surface, forming more distinct channel complexes; these are contained within a background of thin-bedded sandstones and mudstones (Figs 3, 4; Hansen et al. 2017a). Locally (where not removed along the basal erosion surface of the succeeding conglomeratic Stage I), Stage II deposits are overlain by up to 20 meters of blueish mudstone, often with subordinate, very thin-bedded, mudstone-dominated heterolithic sediments, which we refer to as Stage III (Fig. 3). Together Stages I, II and III (where present) we refer to collectively as a *channel complex set*; we adopt this term from the hierarchical scheme of Sprague et al. (2002), which we partly follow, (see Vertical Succession and Architectural Organisation below). A complete channel complex set thus consists of a tripartite, broadly fining-upwards succession (Thompson 2010), which Li et al. (2018) substantiate by Markov chain analysis (Fig. 5). Channel complex sets make up the basic building blocks of the system. This channel system consists of at least four channel complex sets, which are almost vertically stacked (Fig. 3). The axial parts of these have been the subject of detailed studies by Thompson (2010), Tuitt (2015) and Li et al. (2018). The channel complex sets are referred to, in stratigraphic order, as CCS-A to CCS-D.

Thickness of individual channel complex sets varies from about 140 m (CCS-B) to about 50 m (CCS-D), partly as a consequence of variations in the depth of erosion of the base of the channel complex set into the preceding one. The maximum observed depth of erosion associated with the base of Stage I of each channel complex set in the axial region is about 70 m for CCS-A to CCS-C, and about 25 m for CCS-D, and varies laterally, being greatest in what we refer to as the axial region of the channel system (Fig 3). Thus the basal boundaries appear to have a form roughly resembling an inverted Gaussian curve (what might be called the ‘over-easy’ model), though often with a stepped profile in detail. There is a general upwards decrease through the system as a whole in the maximum clast size present in Stage I of each successive channel complex set (generally boulders), but otherwise there is little difference in grain size between successive channel complex sets. Stage I has a slightly higher proportion of coarser-grained (cobble to boulder size) material than Stage II. The proportion of sandstone within Stage I increases from the axis towards the edges of the axial region (cf Campion et al. 2000; McHargue et al. 2011), areas loosely defined here as off-axis.

Stage I.---

Stage I deposits include a wide textural range of conglomerates, from poorly sorted and chaotic to well sorted with clast imbrication, and include both matrix-supported and clast-supported facies (Fig. 6A to F). However, the less organized, mostly clast-supported facies dominate. Grain sizes range from cobble (64 mm – 254 mm) to boulder (≥254 mm), with maximum grain size typically around 300 mm. Conglomerate bodies are discontinuous (in part due to numerous erosion/amalgamation surfaces; Fig. 7), often with substantial and rapid lateral and vertical variations in facies, and are generally impossible to subdivide into individual depositional units (‘channels’ *sensu* Sprague et al. 2002). Continuity tends to increase towards the top of channel complexes, where they can be differentiated (see below). These facies are reminiscent of coarse-grained fluvial deposits (e.g. Miall 1977, 2013), with boulder-size open framework bar cores (Fig. 6A, B), pebbly armor layers (Fig. 6C) and low- to high- angle cross-stratification (Fig. 6D). We interpret these deposits as bed-load generated coarse-grained bars and bed-forms (see below; cf Ito 2019).

Sandstones within Stage I are mostly structureless or weakly stratified (Fig. 6G, H), fine- to coarse-grained, meter-scale lenticular erosional remnants, with discordant upper boundaries formed by the erosional base of the overlying conglomerates (Fig 6A, B, C). These sandstones not infrequently contain large rafts and blocks of thin-bedded material (Fig. 6H). Rarely there are thin (few meters) successions of normally graded sandstone beds with parallel lamination and ripple cross-lamination passing into mudstone tops; these successions form the less-eroded tops of channel complexes (see below). Debrites observed within Stage I are commonly restricted to the basal parts of channel complexes and include both mud-clast-rich and lithic clast-rich (pebbly mudstone) deposits (Fig. 6I). The relative scarcity of debrites is likely due to their erosion by energetic currents within the channel axis.

The basal erosion surface of Stage I (Figs. 3, 4, 7) commonly overlies rotated or deformed thin-bedded heterolithic sediments of underlying Stage II deposits of the preceding channel complex set. At several localities Stage I tops are marked by a laterally continuous body of amalgamated sandstones ≤10 m thick (Figs. 4, 8), marking the transition to Stage II; amalgamation surfaces are commonly marked by discontinuous mud clasts and/or gravel 'stringers'; the basal sections of the thick sandstone packages also contain local scour surfaces filled with granule to small pebble conglomerate.

Stage II.---

Stage II conglomerates are generally finer-grained than Stage I conglomerates (a higher proportion of very coarse pebble material), with grain sizes dominantly ranging from very large pebble (32 – 64 mm) to small cobble (64 ≥ 128 mm) with maximum grain size normally around 200 mm. They are often better organized than Stage I conglomerates, many being very well sorted, with common clast alignment and imbrication, both *a*-transverse and *a*-parallel (Fig. 6E, F). These conglomerate bodies are typically 10 to 15 meters thick, extensive over a few hundred meters to about a kilometer perpendicular to the axial region (Fig. 4) and often contain sets of low-angle inclined stratification, interpreted as lateral accretion surfaces, commonly stacked in several sets through the thickness of one conglomerate body (Fig. 8). The base of any given conglomerate body is in many places marked by a sub-horizontal erosion surface that may be locally stepped (Fig. 8) and occasionally overlies slightly deformed and/or rotated heterolithic beds. Such conglomerates are often overlain by a few meters of sandstone, succeeded by the thin-bedded sandstones and mudstones that form the background sedimentation within Stage II, and encase the conglomerate bodies (Fig. 8). These thin-bedded sediments are dominated by the fine-grained fraction, but locally containing upstream-migrating sandy dune-like features (McArthur et al., 2019). The thin-bedded facies is very similar to that seen in the channel belt margin areas (see below) but also containing near the base of Stage II occasional pebbly mudstones, up to 11 m thick, usually with size and abundance of pebbles decreasing towards the top (Thompson 2010; Hansen et al. 2017a. Also locally present are scattered boulders of basaltic andesite and limestone, up to 5 m across, occasionally with debritic material locally preserved in the re-entrant between the base of the boulder and the underlying thin-beds. The pebbly mudstones are interpreted as debrites. The isolated boulders are interpreted as having been transported either by muddy debris flows (the residue of which is preserved beneath the boulder, the remainder having been eroded away by turbidity currents) or some other high-concentration process.

Stage III.---

Stage III deposits are dominated by mudstones, which include: a dark grey, organic-rich, laminated component interpreted as the deposits of very dilute turbidity currents; pale grey structureless mudstones with local silty patches, inferred to be debrites; and a pale, blue-grey, massive, foraminifera-rich hemipelagite component. They can be distinguished by their distinct palynology and ichnology (see Paleontology section, below). They are often inter-bedded with very thin-bedded heterolithics interpreted as turbidites. We consider these mudstones to represent periodic shut-downs of the channel system and may represent significant periods of time. In some cases they form part of the final channel fill, suggesting that at least some of these deposits plugged the last open channels in the system; poor exposure does not permit the discernment of any vertical trends of grain-size or lithology in these putative channel plugs.

Channel complex sets in axis.---

Channel complex sets represent large-scale cycles of erosion and deposition, within which smaller scale, broadly fining-upward cycles can often be recognized, which we refer to as channel complexes (sensu Sprague et al. 2002, below). Stages I and II of each channel complex set consist of multiple channel complexes (Figs 7, 8). Within Stage I the recognition of individual channel complexes depends on the degree of erosion associated with their bases in any one place. Where the coarsest grained, axial part of a channel complex rests directly on the coarsest grained, axial part of the preceding complex, it is difficult or impossible to distinguish the two. Where this is not the case, the top of a channel complex is often dominated by a continuous sandstone layer that may be of the order of a meter or more in preserved thickness (Fig. 7A, B). Given the difficulty in recognizing channel complexes within Stage I, and their highly amalgamated nature, it is not possible to say with any confidence what their stacking patterns might be.

Within Stage II of the channel complex sets, the distinction between successive channel complexes is generally straightforward where conglomerates are present, the boundary being taken as the erosional base of the conglomerate bodies. The local presence within the thin-bedded sections of bedforms generated by supercritical overbank suggests correlation with active channels. However, channel complex boundaries are impossible to recognize within the background thin-bedded sediments (as in the laterally equivalent thin-bedded sections of the channel belt margins; see below). The conglomerates marking the bases of channel complexes are commonly offset-stacked from one another; nonetheless they are broadly restricted to the axial region of the channel belt (Figs. 3, 4, 8).

Channel belt Margin.---

The channel belt margin is dominated by discontinuously exposed thin-bedded heterolithic deposits with a very irregular bed thickness distribution (Figs. 6J, 9). Thin-bedded heterolithics of any one channel complex set are often directly overlain by similar sediments of the marginal part of the succeeding channel complex set, making the distinction between one channel complex set and the next problematic. However, several condensed sections are present that appear to be equivalent to the tops (Stage III) of channel complex sets in the axis, and where these can be mapped they can be used to establish a general correlation from the channel belt margin towards the axis (Figs. 2, 3). Where these condensed sections are absent, presumably due to erosion, it is not possible to differentiate between channel complex sets in the channel belt margin. Paleocurrent directions show a strong mode parallel to those in the channel belt and to the channel belt itself (Fig. 2). There is generally little evidence of systematic changes within the channel belt margin as one moves laterally away from the channel belt axis (Hansen et al. 2017a); these areas are interpreted as depositional terraces, *sensu* Hansen et al. (2015, 2017b), i.e. more or less flat elevated areas marginal to the active channel, often receiving overbank sediment. Some areas, however, do show a general decrease in proportion of sandstone, average sandstone layer thickness or grain-size, with paleocurrents more divergent from the channel axis, and these are likely to represent internal levees *sensu* Kane and Hodgson (2011), i.e. those that are bounded by an external confining surface (McHargue et al., 2011).

Channel Belt Boundary Zone.---

At the boundary between the channel belt margin and the external levee (see below) is a transition zone, typically around 200-400 m wide, characterized by the local presence of large (tens of meters or more in lateral extent) regions where bedding dips are of scattered azimuth, and steeper (from 30 to 80 degrees) than the regional dip (Dykstra and Kneller 2007; Hansen et al. 2015; Hansen 2016; Hansen et al. 2017a), with facies resembling those of the proximal external levee (Kane et al. 2007). These are surrounded by sediments with regional dip (Hansen et al. 2017a). For all practical purposes it is impossible to identify a discrete boundary between the channel belt margin and the external levee except by virtue of the change from consistent to variable dips. Exposure is insufficient to define this in detail.

External Levee.---

The external levee has been described in detail by Kane et al. (2007), Hansen et al. (2015), Hansen (2016), and Hansen et al. (2017a). Logged sections in the external levee demonstrate lateral bed thickness variations and changes in ichnofacies and palynofacies (Kane et al. 2007; Callow et al. 2013; McArthur et al. 2016; Hansen et al. 2017a; see below).

The external levee consists of very regular, non-amalgamated sandstone-mudstone couplets (Figs 6K, 9A). These are generally ≤20cm thick, decreasing away from the channel belt, with a sand content of approximately 50% close to the channel belt, dropping to about 5% in the very thin-bedded couplets of the distal levee 3km from the channel belt (Fig. 9A). Both bed thickness and proportion of sand decay away from the channel belt according to a power law (Fig. 9D; Kane et al. 2007; Hansen et al. 2017a; see also Birman et al. 2009; Nakajima and Kneller 2013). In the proximal part of the levee the sands are often normally graded in the upper part and with climbing ripples, commonly with an abrupt break between the sand and silt-to-mud portions of the bed, whereas in the distal parts of the levee the sands commonly consist of starved ripples. The mode of the sand grain-size distribution decreases from c. 120 μm in the most proximal part of the levee to c. 65 μm in the distal area, but the sand becomes siltier distally, the grain-size distribution acquiring a longer fine-grained tail (Fig. 10A).

These alternations of sandstone and mudstone are interpreted as overbank turbidites. The thinning and decrease in sand content of levees from proximal to distal areas is often considered diagnostic of levees (e.g. DeVries and Lindholm 1994; Hiscott et al. 1997; Migeon et al. 2000). The common sharp tops to the sandstone component of the turbidites in the proximal levee may be due to the missing grain-sizes having bypassed to more distal parts of the levee (Kane et al. 2007; Hansen 2016; Hansen et al. 2017a) or possibly having been removed by clear-water bottom currents. In some localities proximal to the channel belt there is a weak paleocurrent mode roughly parallel to the channel belt (and to the inferred levee crest), but paleocurrent directions in the levee overall are largely towards the SSE. This may indicate the presence of topographic complexities on the external levee (Hansen et al. 2015; Hansen 2016) or that the external levee sediments were reworked by contour currents (Stow et al. 2013; see below).

PALEONTOLOGY

Biostratigraphy

Palynological biostratigraphic analysis was conducted on fifty-one samples collected throughout the system, utilising first occurrence, last occurrence and acme zones previously defined onshore and offshore Mexico (Helenes 1984; Helenes and Téllez-Duarte 2002) and the USA (Firth 1987 1993; Lucas-Clark 2006; Dastas et al. 2014). Here we summarise the more detailed account in McArthur et al. (2016).

Dinoflagellate cyst biozonation of the Upper Cretaceous is low resolution, simply dividing the stages into upper and lower zones. Nonetheless a rudimentary biozone scheme is erected.

Samples from the channel system underlying the San Fernando indicate a Lower Maastrichtian age. A single sample from a muddy debrite at the base of CCS-A indicates an Upper Maastrichtian age. Since debrites can only rework older material, an Upper Maastrichtian age can be taken as the oldest possible for this interval.

Numerous samples from CCS-B contain biostratigraphically important Maastrichtian dinocysts markers such as *Hafniasphaera fluens* and *Xenascus ceratioides*, but are generally dominated by simple, proximate forms. CCS-C continues to show Maastrichtian marker species. Samples from the lower portion of CCS-D are the last to show Upper Maastrichtian marker species. A barren zone occurs within the uppermost hemipelagic section, that marks the Cretaceous – Paleocene boundary. Samples from the overlying succession contain Danian marker speciesand lack the previously abundant Maastrichtian markers. A distinct change in the terrestrial palynomorphs is also observed, with samples in CCSA-D containing abundant Mesozoic pollen and spores, which are absent above the barren zone.

Although samples from the external levee were productive, they simply yield an Upper Maastrichtian assemblage, thus correlating with CCS-A through to CCS-D.

Palynology

Palynofacies analysis of channel belt axis samples shows well-sorted assemblages of particulate organic material, dominated by humic, woody debris, which often shows evidence of mechanical damage and fragmentation (McArthur at el. 2016). Particles range up to 375 μm, averaging 43 μm and are typically rounded and spheroidal.

Lighter plant debris, palynomorphs and amorphous organic matter are very rare and are interpreted to have bypassed to overbank or down-fan environments (McArthur et al. 2016).

Channel belt margin palynofacies samples have poorly sorted assemblages of organic matter, mixing terrigenous and marine particles. Phytoclasts are typically rounded but smaller than in the channel belt axis, with maximum size of 128 μm and an average of 34 μm. Miospores, though rare, are small (<30 μm) and smooth (McArthur et al. 2016).

The most proximal parts of the external levee (including the channel belt boundary zone) exhibits the most poorly sorted palynofacies assemblages dominated by equant opaque phytoclasts, degraded wood, amorphous organic matter, cuticle and bladed opaque phytoclasts, with the greatest abundance of palynomorphs (McArthur et al. 2016). Phytoclasts are typically sub-angular and sub-elongate, up to 75 μm long, averaging 28 μm.

Palynologically the outer external levee displays higher levels of autochthonous, marine material and lesser terrestrial debris compared to the inner external levee. In addition to increased amorphous organic matter, counts of dinoflagellate cysts are the highest for any sub-environment. Phytoclasts are typically sub-angular, sub-elongate and their size diminishes moving away from the channel belt, reaching a maximum of 65 μm and averaging <20 μm (McArthur et al. 2016).

Hemipelagites show well sorted palynological assemblages, dominated by amorphous organic matter, though still with moderate proportions of phytoclasts, typically sub-angular and elongate, with maximum size of 48 μm, averaging 12 μm (McArthur et al. 2016).

Detrended correspondence analysis of the palynofacies reveals gradational groupings, corresponding to channel belt axis, channel belt margin, inner external levees, outer external levees (see External Levee section) and hemipelagites (Fig. 11).

Ichnology

Phycosiphoniform/*Chondrites* ichnofabrics (sensu Callow et al. 2013, i.e. *Phycosiphon, Planolites, Chondrites*) occur across the entire channel belt (Kane et al. 2007; Callow et al. 2013; Fig. 12A). However, the channel belt margin samples, especially those distal to the channels belt axis, have characteristic and dominant *Scolicia* ichnofabrics (Fig. 12B, C), with accessory phycosiphoniforms (Fig. 12D), *Nereites* (Fig. 12E) and *Ophiomorpha*. (Fig. 12F) Interface trace fossils are common on the bases of sandstone beds, including *Paleodictyon isp*. *Megagrapton irregulare*, cf. *Belorhaphe isp*. *Cosmorhaphe isp*. *Protovirgularia isp*. *Spirorhaphe involuta*, *Helminthorhaphe isp*. and *Desmograpton isp.* (Callow et al. 2013).

Trace fossils in the axial region of the system are restricted to an *Ophiomorpha* ichnofacies association (*Ophiomorpha*, *Phycosiphon*, *Chondrites*), and may also contain the deep, paired, sand-filled burrows of *aff. Tisoa* (Fig. 12G; *Diplocraterion* of Hubbard and Schultz 2008), which is characteristic of the firm-grounds associated with bypass surfaces; this is found only in the axial region of the channel belt (Callow et al. 2013), whereas the *Ophiomorpha* ichnofacies association is also found in the adjacent overbank regions (see below).

A *Nereites* ichnofabric association (*Nereites*, *Phycosiphon,* rare examples of *Zoophycos* and *Spirophyton*, and may be associated with the *Pilichnus*, *Nereites*, *Phycosiphon* and *Lophoctenium* ichnofabrics) occurs within outermost terrace and levee environments (Kane et al. 2007; Callow et al. 2013), with accessory *Planolites* and *Zoophycos*. Aggregates of the benthic foraminifera *Bathysiphon* are also present.

Associations of *Lophoctenium*, *Phycosiphon,* and *Nereites* occur in mid to distal levee settings. The distribution of ichnofacies associations is distinctive, and allows the differentiation of different parts of the channel system (Fig. 11E).

PROVENANCE

Detrital zircon ages are similar to those published by Sharman et al. (2015), with a peak of ~90-100 Ma, consistent with the 90-97 Ma zoned tonalite to granodiorite La Posta plutons of the eastern Peninsular Ranges Batholith (Gastil et al. 2014). A minor component of mid-Jurassic zircons (~166 Ma; Sharman et al. 2015), probably related to older arc rocks further to the east, increases stratigraphically upwards. Sandstones are mostly feldspathic litharenites falling within the dissected arc field of Dickinson, (1985) (Fig. 10). Clasts are composed mainly of porphyritic and aphyric felsic volcanic rocks (rhyolite/dacite), rhyolitic welded tuff, and sandstones, with subordinate felsic and mafic plutonic rocks, and scarcer metamorphic rocks. The coarsest fraction consists almost exclusively of crystalline rocks. Conglomerates are dominated by clasts of pyroclastic, porphyritic and aphanitic volcanic rocks with very subordinate sedimentary and metamorphic clasts. The maximum average grain-size within each CCS decreases slightly upwards, along with a very slight decrease in the proportion of pyroclastic rocks. Heavy minerals show little change stratigraphically within the channel belt. However, the external levees are enriched in apatite and tourmaline, the lowest density of the heavy mineral phases.

CHANNEL GEOMORPHOLOGY AND PROCESS

Here we attempt to define the form of depositional elements and the processes occurring within them, in order to construct a series of models for the morphology of the channel system at the sea floor as it evolved through time.

Channel belt axis

Stage I.---

In Stage I, the dominance of clast-supported, usually poorly organized conglomerates indicates bed-load transport beneath powerful turbidity currents flowing within channels. The depth and width of the channels, and whether only one or several channels were active at any one time, is a matter of speculation. Nonetheless, they are likely to have been at least as wide as the flow-normal width of erosion surfaces that bound individual units of fill (many tens of meters), and as deep as the depth to which these surfaces incise into the underlying succession (at least of the order of 10 m); these values are consistent with the sizes deduced by McHargue et al. (2011) for their ‘filled channel elements’ (width 200-300 m, depth of the order of 10 m). These erosional features are, however, substantially smaller than the dimensions of many channels on the modern sea floor (Konsoer et al. 2013), which vary widely but appear rarely to be less than 100 m wide, and commonly a kilometer or more, while erosional channels have depths generally exceeding 20 m, and widths up to several hundreds of meters (e.g. Dalla Valle and Gamberi 2011; Gamberi and Marani 2011; Maier et al. 2012). The dimensions that we identify (above) for individual erosion surfaces, and which accord with those of filled channel elements, are more consistent with the sizes of individual scours within channels (Normark et al. 1979; Malinverno et al. 1988; Hughes-Clarke et al. 1990; Shor et al. 1990), having depths of tens of meters and lengths of ≥100 m. This suggests that the channel itself may have been far larger, perhaps on the scale of the entire channel complex set incision (of the order of several tens of meters deep and 2 to 4 km wide), albeit perhaps with multiple thalwegs.

In Stage I, the original form of the channels is thus far from clear, but we suggest they contained analogous elements to those seen in braided river systems (Miall 1977, 2013; Lunt and Bridge 2004; Bridge 2006), including multiple types of bars and large gravel bedforms (Piper and Kontopoulos 1994) such as gravel dunes with wavelengths mostly from 40 to 70 m, and gravel waves with amplitudes up to several meters and wavelengths up to several hundred meters (Malinverno et al. 1988; Hughes Clarke et al. 1990; Kidd et al. 1998; Morris et al. 1998; Wynn and Stow 2002; Paull et al. 2010; Gamberi and Marani 2011; Migeon et al. 2012). These would be associated with extremely large turbidity currents such as the Grand Banks event of 1929, and the 1979 event in the Var submarine canyon (Piper and Savoye 1993; Malinverno et al. 1988). Multiple sub-parallel low sinuosity channels or thalwegs may have been present, as seen in some modern systems (e.g. Stromboli channel; Gamberi and Marani 2011).

Thus for Stage I of each channel complex set we envisage a single broad channel or braid-like pattern of channels, with various types of bar and bedform such as gravel waves, flanked by eroded hemipelagic slope sediments on the SE, and by terraces on the NW (Fig. 3). The terraces received suspended sand and mud falling out of suspension from currents that were largely bypassing the channels, and which extended across the entire channel belt; these flows were capable of moving gravel as bed-load within the channels. Although it is unclear what was the elevation of the terraces above the thalwegs of the channels, in modern systems this is typically of the order of tens of meters (e.g. Babonneau et al. 2010; .Maier et al 2013; Gamberi and Marani 2011), and even coarse sand may reach the terraces. Some of these flows were probably contributing sediment to the levees also. A corollary of this is that at least some of the terrace deposits must be time-equivalent to Stage I in the axis (Fig. 13).

There is thus virtually no possibility of establishing time-correlative surfaces between the channel belt axis and the terraces.

Stage II.---

The transition to Stage II appears to coincide with the filling of the accommodation created by the erosion at the base of the channel complex set (inner confinement *sensu* McHargue et al. 2011), to which the coarser-grained bodies of Stage I are confined (Fig. 3, 13). The flows occurring after this erosional relief had been filled would have been substantially less confined and therefore, all other things being equal, weaker than those lower in Stage I, probably explaining the absence of coarse bed-load deposits since any gravel would have been deposited further upstream, resulting in the local presence of a continuous sandstone unit at this transition (Figs. 3, 4).

The geometry of Stage II channel fills as laterally continuous, more or less sheet-like bodies of conglomerate (typically capped by sandstone; Fig. 8), combined with lateral accretion sets, suggests that they were formed by sinuous channels, generating meander belts of the order of a kilometer wide, with little or no aggradation occurring during their migration (Figs. 4, 8; Clark et al. 1992; Peakall et al. 2000, 2012; Abreu et al. 2003; Posamentier 2003; Kane et al. 2009; Dykstra and Kneller 2009; Janocko et al. 2013; Li et al., 2018). The generally very well-sorted and imbricated gravels contained within them (Fig. 6D, E, F) suggest substantial bedload transport by somewhat less energetic currents than those of Stage I, and possibly less catastrophic. Both sliding (traction carpet) and rolling modes of bedload transport are indicated by the presence of both *a*-parallel and *a*-transverse clast fabrics. The Stage II channel fill bodies are substantially thinner than the inferred thickness of the currents required to move the channel-filling gravel, implying substantial flow over the adjacent terrace regions (as argued by Dykstra and Kneller 2009). The fluid mechanics of stratified flows would suggest that the lower part of the flow may be confined to (and follow) the channel (Kneller and Buckee 2000), while the upper part followed the mean direction of the channel belt.

Orders of magnitude for Stage II maximum channel depth may be estimated from the thickness of lateral accretion sets plus the overlying sand bodies (approximately 15 m in total). The minimum channel width may be indicated by the dip length of the lateral accretion sets (of the order of 50 m). This is small compared to most modern meandering submarine channels (Pirmez et al. 2000; Abreu et al. 2003; Deptuck et al. 2007; Babonneau et al. 2010), and almost certainly far smaller than the channels in Stage I. Multiple channel storeys (Fig. 8B) indicate a protracted history of channel migration, with multiple meanders passing the same point during evolution of the meander belt.

Stage II meandering channels appear to have been flanked on both sides by terraces (Figs. 8, 10). None of the Stage II conglomerate bodies show significant aggradation. This suggests that the channels were at grade (no changes in flow parameters with time; Kneller 2003), and that channel activity was switched on and off by some external forcing. The thin-bedded intervals stratigraphically between the channels may thus represent either partial shut-down of the channel system (but with significant aggradation), or depositional terrace/internal levee deposits (Li et al. 2018; Figs. 8, 13 lateral to highly aggradational channel bodies that are poorly-exposed or indiscernible (perhaps sand or mud-filled). Such transition from graded sinuous to highly aggradational channels has been documented in, for example, the shallow subsurface of the Bengal Fan (Kolla et al. 2012), and Makassar Strait, Indonesia (Posamentier and Walker 2006).

Stage III.---

Stage III represents extended shut-downs of the channel system, where no substantial flows were passing down the channel belt. This is reflected in the fact that Stage III is dominated by marine organic material (see below), whereas Stages I and II are dominated by terrestrial material (McArthur et al. 2016).

Channel Belt Margin.---

The channel belt margin sections have been described in detail by Hansen (2016) and Hansen et al. (2017a). These heterolithic sediments (dominantly thin-bedded turbidites) are interpreted to be depositional terraces (*sensu* Hansen et al. 2015) or internal levees adjacent to the channels, upon which sedimentation occurs as the result of flow that is not confined within the channel axis but extends across the outer confinement (*sensu* McHargue et al. 2011). This is defined in the east by the surface of incision into slope sediments, and on the west by the inner slope of the external levee.

In Stage I of CCS-A these terraces appear to have been restricted to the NW part of the channel belt. The higher channel complex sets appear to have extensive terraces on the SE side, but poorer exposure here precludes the differentiation of the terraces of one channel complex set from another with any confidence. In Stage II, sediments interpreted as depositional terraces occur widely across the entire channel belt, suggesting that terraces occurred on either side of the meandering channels which at any one time occupied only a limited width of the channel belt.

Heterolithic channel margin regions also include discrete scour-based, fining-upwards packages (up to pebbly sandstone at their bases) that we interpret as the fills of chute channels (Hansen 2016). Chute channels (Miall 1977, 2013) in both modern (Gamberi and Marani 2011) and ancient deep-water channel systems (Hein and Walker 1982) may occur both on bars within the channel belt and on the terraces, where they typically develop in overbank areas that are only slightly elevated (< 20 m) above the adjacent active channel (Hansen 2016). These chute channels preferentially transport coarser material than that on the surrounding bar or terrace as they are topographically lower. Chute channel fills almost certainly exist also within the Stage I channel fills but we are unable to recognize them.

Areas where the thin beds in the channel belt margin show systematic changes in bed thickness and proportion of sandstone away from the channel axis are interpreted as internal levees, *sensu* Kane and Hodgson (2011). Bed thickness distribution in these areas tends to be more variable than in the external levee (Hansen et al. 2017a).

Channel Belt Boundary Zone.---

Blocks of more steeply dipping material in the region between the channel belt margin and the external levee are interpreted as displaced blocks of external levee material that have collapsed from inner regions of the levee. Many shallow seismic and sea floor examples illustrate the complexity of these channel belt boundary zones (e.g. Deptuck et al. 2003; Migeon et al. 2006; Dykstra and Kneller 2007; Sawyer et al. 2007; Hansen 2016; Hansen et al. 2017b).

External Levee.---

The levee is by definition a geomorphic element that, based on many modern and ancient examples, can be divided into an inner and outer region, separated by the levee crest (e.g. references cited in Kane and Hodgson 2011). Inner external levee slopes facing the channel belt are generally steeper – often considerably so – than the outer external levee, often cut by arcuate slide scars due to collapse into the channel belt (as seen here in the channel belt boundary zone). The outer external levee generally has a gradient that progressively declines distally (Pirmez et al. 1997; Hübscher et al. 1997; Droz et al. 2003; Migeon et al. 2006; Nakajima and Kneller 2013). The more proximal part of the outer external levee not infrequently has constructional features such as long wavelength (~1 km) sediment waves (e.g. Migeon et al. 2000, 2006; Wynn and Stow 2002), but if present in this system we have been unable to recognize them (Hansen et al. 2017a). The regularly-bedded sediments of the external levee are interpreted as the deposits of turbidity currents that were thick enough to over-top the crest of the levee.

Clearly such currents must also have flowed over the terraces within the channel belt; these would have received deposition from the lower (higher concentration, coarser grained) parts of flows. Of course, the converse is not true (i.e. that flows that deposited on the terrace also deposited on the external levee), thus the height of the levee effectively constitutes a filter on the size of turbidity currents (flow scaling of McHargue et al., 2011) that can deposit sediment on the levee beyond the levee crest. Some flows would be confined to the channel belt while others were not. Modern levees may have heights well in excess of 100 meters (e.g. Amazon Fan, Damuth et al., 1995; Congo Fan, Babonneau et al., 2002), and in extreme cases greater than 300 meters (Piper & Savoye, 1993), but since in San Fernando there are no correlatable surfaces from the channel belt into the levee it is not possible to constrain their height.

The relative timing of levee growth and the stages of evolution of the channel belt fill are similarly unknown. It is reasonable to suppose that levee growth occurred during the passage of the thickest flows, but these may not necessarily have been the largest, most energetic or most coarse grained, as is illustrated by the Var system in which thicker and slower-moving, muddy flows which produce deposition on the levees alternate with thinner, faster, sandy flows which do not (Khripounoff et al. 2012).

Flow properties

To provide order of magnitude estimates of the flow parameters for turbidity currents able to move the observed grade of sediment as bedload, we compare an estimated dimensionless shear stress Θ with an estimated boundary Reynolds number to determine whether the shear stress exceeds the threshold of motion (Shields 1936):

$$\Theta = \frac{\tau_0}{(\rho_s - \rho) g D}$$

where ρ_s is sediment density, ρ is ambient water density, τ_0 is shear stress (given by $ghS\Delta\rho$ where $\Delta\rho$ is the excess density of the turbidity current and S is the slope), and D is particle diameter. The shear stress thus increases with slope, excess density and thickness of the current.

The boundary Reynolds number is given by:

$$\mathrm{Re}_* = \frac{u_* D \rho}{\mu}$$

where u_* is shear velocity = $\sqrt{\frac{\tau}{\rho}}$ and μ is dynamic viscosity (Allen 1984; Middleton and Southard 1984; van Rijn 1993).

Reasonable ranges of slope, and thickness of the current can be estimated from modern systems. Gradients of slope channels and canyons on active continental margins tend to be in the range 1.5 to 4°. Orders of magnitude for flow thickness can be estimated from large historic events; the 1979 event in the Var Canyon reached an estimated thickness of >120 meters (Piper and Savoye 1993), the 1929 Grand Banks event is estimated to have been between 270 and 420 meters thick (Piper et al. 1988), and currents within the Congo Canyon are of the order of 45 to 150 meters thick (Andrieux et al. 2013; Azpiroz-Zabala et al. 2017). Excess density is a function of suspended sediment concentration, measurements of which are extremely sparse, but Xu et al. (2013) report maximum values of 60 kg m^{-3} from currents in the Monterey Canyon, and possible as much as 275 kg m^{-3} in the basal layer (Wang 2018). Since suspended sediment concentration and velocity both decay upwards (e.g. Garcia and Parker 1991; Sequeiros et al. 2010) depth-averaging would yield smaller values for thickness.

Since the largest clasts tend to occur in more chaotic or structureless deposits, which may have been emplaced by debris flows and subsequently winnowed by turbidity currents, we take as an indicative particle diameter the typical size of well-imbricated clasts that we can be confident were transported as bedload, namely about 0.1 m. Adopting highly conservative values for flow thickness (20 meters), excess density (40 kg m^{-3}) and a gradient of 1.5° yields a boundary Reynolds number Re* of 1136, and a Shields parameter Θ of 0.129, which is well in excess of the movement threshold for these clasts using the extended Shields diagram of Miller et al. (1977). The critical bed shear stress required to move gravel over the bed will be increased in the presence of bedforms, which would introduce form drag (Dietrich and Whiting 1989), but the shear stresses calculated here are substantially in excess of the threshold. In fact the gradient of this channel system was probably closer to 4° based on the depth estimates and the distance to the shoreline, so these are extremely conservative estimates.

Many of the conglomerates within Stage I (especially in CCS-A) are very much coarser than 0.1 m, implying substantially larger currents. This suggests that the flows responsible for the majority of the Stage I and all of the Stage II fills may have been considerably thicker than the depth of the channels through which they flowed and would have occupied much of the channel belt. This implies very substantial flow over (and deposition on) the terraces of the channel belt margin, especially since we have adopted an integral value for the flow depth whereas in reality the density structure of turbidity currents shows an upward decline in suspended sediment concentration (e.g. Garcia and Parker 1991, 1993), accompanied by a decrease in maximum grain-size (e.g. Garcia 1994).

Sediment bypass.---

The conglomeratic facies undoubtedly represent very substantial bypass of sediment through the system (Hubbard et al. 2014; Stevenson et al. 2015). The driving force for the turbidity currents moving the gravel as bed-load is gravity acting upon the suspended sediment, little of which was deposited at this locality. In fact the erosion surfaces at the base of the channel complex sets represent complete bypass without any net accumulation of bed-load material (see below). Occasional remnant lenses of coarse-grained sandstone within the Stage I deposits, the interstitial sand within the conglomerates, and more continuous beds at the Stage I/II boundaries, give some indication of the nature of the coarser fraction of the material being carried in suspension.

As an order of magnitude illustration of the bypass potential of this system (see also Stevenson et al. 2015), a flow with the properties illustrated above, travelling at 10 m s^{-1} (e.g, Malinverno et al. 1988; Hughes Clarke et al. 1990) through a channel 100 m wide would deliver roughly 30×10^9 kg of sediment to the basin over the course of a 10 hour flow. Allowing for 30% porosity, this is enough to create a 10 cm thick bed with an area of roughly 140 km^2. Given that the deposits of each channel complex set, especially during Stage I, represent many hundreds to thousands of flows, this represents a considerable transfer of sediment downslope, especially when considering the sediment that bypasses during cutting of the bounding surface when no deposition at all occurs within the channel.

Topographic interaction.---

Flow stratification is implicit in the structure of turbidity currents, but the degree and nature of stratification depends both on the shear velocity of the flow (see above) and the grain-size distribution of suspended sediment (Middleton and Southard 1984; Garcia 1994). Where the coarsest grains are far from their suspension threshold, as in the largest and fastest flows, the density gradient near the base of the flow will be small. In this case the flow will be relatively unresponsive to the channel topography (Baines 1995; Kneller and Buckee 2000). Coarse suspended sediment will be dispersed over a larger height above the bed than in smaller, slower flows, and substantial quantities of the coarser suspended sediment will spill onto the over-bank regions, including the terraces in the channel margin. Conversely, in less energetic flows, in which the settling velocity of the largest grains approaches the shear velocity of the current, the base of the current will be well-stratified, and will respond to (and may be confined within) topography such as channel margins (Kneller and Buckee

2000), inducing behavior more like that of fluvial systems (Dykstra and Kneller 2009) and perhaps explaining the fluvial-like architectures of Stage II channel fills.

VERTICAL SUCCESSION AND ARCHITECTURAL ORGANISATION

A number of architectural schemes have been proposed for the stratigraphic organization of slope channel systems, including Mayall and Stewart (2000), Sprague et al. (2002) and McHargue at al. (2011). One feature these models have in common is cycles of waxing and waning energy at a range of scales, from that of the whole system down to that of channel elements in the McHargue et al. (2011) terminology, or 'channels' in the Sprague terminology—which we eschew on the grounds that the deposits rarely if ever reflect the form of the channel as it existed on the sea floor. These result in a hierarchy of fining-upwards sequences that is common to all these architectural schemes; differences in detail between these schemes possibly reflect the differences between the range of systems studied by each of these authors. In fact such cycles of erosion followed by fining-upwards channel fills have been a common observation for some decades (e.g. Mutti and Ricci-Lucchi 1972).

Our observations of the San Fernando channel system accord well with the scheme of Sprague at al. (2002, though the data on which their scheme was based have not been published), but the vertical scale of the San Fernando system (c. 400 m) is significantly larger than in their scheme (of the order of 100 m). Nonetheless, we have adopted their hierarchy, with some minor adjustments to nomenclature as above (Fig. 3). Overall the channel complex sets become on average somewhat finer-grained up-section, and the youngest channel complex set is less incised than any of the underlying ones. Individual channel complex sets themselves represent crudely fining-upwards sequences, with the coarsest material (boulder size) being present (though scattered) near the base of Stage I. (Note that this does not include the anomalously large boulders.) The degree of amalgamation and entrenchment changes in a more stepwise fashion at the Stage I to II boundary rather than being progressive, with the change from straighter or perhaps more braid-like channel forms to meandering forms, being related to changes in confinement, flow properties and possibly in part to the presence of more cohesive bank material (Audet 1998; Peakall et al. 2000). At the scale of the channel complex (where they can be differentiated), each successive channel complex tends to be finer-grained than the preceding one, in both Stage I and in Stage II.

Stage I of our channel complex sets resembles the 'filled channel element', of McHargue et al. (2011) but on a seemingly larger scale. Note that the schemes of McHargue et al. (2011), and Mayall and Stewart (2000), though broadly similar to ours, have one less level in the hierarchy than the scheme presented here and by Sprague at al. (2002), perhaps because the smallest scale that is resolvable in the subsurface is typically that of the channel complex set ('channel complex' of Mayall et al. 2006).

McHargue et al. (2011) also describe 'inner confinement' corresponding to our Stage I bounding erosion surface, and 'outer confinement' that equates to the bounding topography of the entire channel belt (levee to the NW and slope to the SE; Fig. 3). Between these two is the area occupied by terraces, which are nonetheless aggradational, possibly even when the Stage I bounding surface (inner confinement) is being cut.

Cycles of erosion and deposition essentially represent re-grading of the channel in response to changes in flow parameters (Pirmez et al. 2000; Kneller 2003). During phases of increasing flow magnitude the equilibrium gradient of the flow will decrease, resulting in erosion of the channel floor. The fill is generated as decreases in flow magnitude result in steepening of the equilibrium gradient with consequent generation of accommodation. Thus a significant proportion of the time during which the channel was active is wholly unrepresented in the channel fill, and this is true at all scales.

Sequence stratigraphy

The scale of an entire slope channel system is typically that of a 3rd order sequence (e.g. Mayall et al. 2006; McHargue et al. 2011). Since the succession immediately underlying the San Fernando channel system is of Lower Maastrichtian age, the San Fernando is Upper Maastrichtian and is immediately overlain by Paleocene sediments, it would appear to represent a single 3rd order sequence, as suggested by Dykstra and Kneller (2007). Thus each channel complex set broadly represents a 4th order cycle. In terms of sediment delivery down-dip, channel complex sets and their basal erosion surfaces would probably be equivalent to lobe complexes *sensu* Prélat et al. (2010) on the basin floor (Johnson et al. 2001), each representing a few hundred to a few thousand flows. The channel complex set deposits themselves would be correlative of retrogradational phases of the lobe complexes (Hodgson et al. 2016.

The system represents repeated cutting and filling at a range of scales. At the largest scale, a large fraction (perhaps half) of the duration of a 3rd order cycle is bound up in the formation of the composite bounding erosion surface, with the majority of the sediment transfer to the basin floor during the entire 3rd order cycle occurring during erosion of the bounding surfaces and deposition of Stage I. At each successively smaller scale a similar fraction of the time is represented solely by erosion, with no sediment preserved in the channel, except perhaps as a lag. Thus it is likely that the Stage I and Stage II fills represent substantially less than half of the lifetime of the channel.

HYDROCARBON RESERVOIR POTENTIAL

Many of the published models for slope channel architecture have been developed with hydrocarbon reservoir analogues in mind (e.g. Mayall and Stewart 2000; Camacho et al. 2002; Sprague et al. 2002; Beaubouef 2004; Barton et al. 2010; McHargue et al. 2011; Macauley and Hubbard 2013). The architecture shown here gives some insights into potential reservoir distribution in such coarse-grained systems, which form active reservoirs offshore Brazil (e.g. Viana et al. 2003) and Angola (e.g. Sikkema and Wojcik 2000). In the highly amalgamated Stage I deposits, connectivity and the absence of baffles or barriers would make for good reservoir, although the facies and permeability heterogeneities within Stage I would tend to generate preferential pathways for fluid migration in the coarser facies, possibly leading to water break-through. The presence of pervasive calcite cement in the sands that make up the matrix of the conglomerates in this specific example would detract from reservoir quality. The channel bodies in Stage II, while laterally extensive, could be stratigraphically isolated from one another, given the nature of the intervening thin-bedded sections. The thin-beds of the depositional terrace areas and the external levees together contain a high proportion (perhaps >50%) of the net sand within the system. Communication between the Stage I channel fills and the correlative thin-beds of the terraces is likely, though the permeability differential would probably lead to bypassing of the thin beds.

Seismic detection of these depositional elements would depend on the frequency of the data, but simple convolution models (e.g. Szuman 2009) suggest that detection of channel complex set boundaries in vertical sections is unlikely in 30-40 Hz data. It may be feasible in higher frequency data (>60 Hz) or in horizon slices, though less likely in the axial region, where the Stage I of successive channel complex sets may be amalgamated (Szuman 2009; Zhang 2013).

Resolution in well data would depend upon the exact position of the well with respect to the channel belt, and the stacking of the channel complex sets (e.g. Barton et al. 2010; Li 2017 and Li et al. 2018). Complex architectures are possible where depositional terrace bodies are founded on earlier channel fills, potentially leading to spurious interpretations of large scale channel migration (Hansen et al. 2016).

DISCUSSION AND CONCLUSIONS

This system has features in common with (and differences from) published architectural schemes based on outcrop and/or subsurface data. As with many other slope channel systems the fill is organised into broadly fining upwards and progressively less erosive cycles. The basic building block is a channel complex set (4^{th} order) that evolves with time from amalgamated coarser-grained channel fills (Stage I) to slightly finer-grained sinuous channel fills that form stratigraphically isolated bodies (Stage II) embedded in thinner-bedded, finer grained background material. Stage I of a channel complex set is underlain by an erosion surface, the coarse-grained amalgamated fill of which is laterally equivalent to and contemporaneous with terraces in the channel belt margin that lies between the axial region and the external levee. The erosional confinement of Stage I possibly represents the width of the coarse-grained channel as it existed on the sea floor; smaller scale elements of published architectural schemes probably represent scours, megaflutes and subsidiary thalwegs within these much larger channels.

Sub-environments on the contemporaneous sea floor can be recognized from the depositional elements. From these it is possible to reconstruct the evolution of the channel system through time. Each channel complex set began with erosion in the center of the channel axial region, leading to complete bypass. As the channel re-graded with diminishing flow size and/or density the fill began to aggrade as bedload on a coarse-grained, probably braided channel floor with gravel bars and bedforms (comparable to the floors of modern coarse-grained slope channels), though still with a large amount of bypass of suspended sediment. The large flows produced contemporaneous deposition on the adjacent terraces outside the axial erosion surface but probably also on the external levee. As in modern systems, smaller and finer grained turbidity currents were probably frequent, producing finer-grained deposits on the depositional terraces which were not preserved in axial areas.

As the axial (Stage I) erosion surface filled, flows became less confined. This was probably superimposed on a long-term decrease in flow size, and perhaps also an increase in mud content. Together these effects led to a change of channel style to a more meandering habit, but notably with no aggradation, indicating that the channels were at grade, with little change in flow parameters over the time-scale of formation of one meander belt. Vertical isolation of these channel fill bodies suggest an external (5^{th} order) cyclicity in sediment supply and/or flow size, but the repeated alternation between graded and aggradational channels is enigmatic. Possibly less (if any) sediment reached the external levee at this time since flow sizes were smaller, though terraces or internal levees would have been receiving sediment from overbanking flows. The majority of the time when the channel system was active as a sediment conduit is not represented in the fill, and this is almost certainly the case with most slope channel systems. The bulk of the sediment that was delivered to the system passed through it with no deposition, to feed lobes or confined sheet systems further down-dip.

Substantial thicknesses of thin-bedded turbidites were deposited as external levee, depositional terraces (*sensu* Hansen et al. 2015, 2017b), and internal levee and/or abandonment deposits. Terraces have a much higher standard deviation of sandstone layer thickness than both external levee and mud prone internal levee/abandonment deposits (Fig. 9A), but can also be differentiated based on the presence of their distinctive *Scolicia*-dominated trace fossil assemblage (Fig. 11A, E). The difference in maximum grain-size and the segregation of heavy minerals between the terraces and external levee both bear witness to the grain-size stratification of the flows.

Overall, organic material passing through the system was sorted by weight (larger, denser material being confined to the axial region), allowing differentiation of sub-environments (McArthur et al. 2016; Fig. 11B). Terrestrial organic material in the external levee decreases away from the channel belt, indicating the declining influence of over-spilling turbidity currents down the levee.

Differences in ichnology from one part of the system to another (Fig. 12; Callow et al. 2013) are reflective of differences in current energy, oxygenation and supply of organic material. The channel belt tends to be better oxygenated due to the action of clear water currents, including the internal tides and waves that are virtually ubiquitous in the modern ocean, and for much of the time are the dominant currents within slope channels and canyons. Modern slope channels and canyons are hot-spots for biodiversity as a result of such currents, which maintain suspended nutrients in dilute nepheloid layers. These effects are optimized on the depositional terrace areas where the shallower-burrowing infaunal echinoid responsible for the *Scolicia* trace survived well, protected from the most energetic currents along the channel axis, where only deep-burrowing infauna survive. The outer external levee environment grades into the background slope with increasing distance from the channel, being more oxygen-depleted, with only shallow-tier grazing traces such as *Nereites*, and organic material increasingly dominated by pelagic fall-out as the supply of terrestrial material in overbanking flows diminishes. Current directions on the levee are widely dispersed (see also Kane et al., 2007) but almost entirely within the range from ESE to SW, with a majority in a generally southerly direction. This distribution, generally parallel to the slope, as well as the common abrupt grain-size break at the top of the sandstones in beds of levee sediment, and starved ripples in the distal levee, suggest the action of low-velocity geostrophic currents reworking and partially winnowing the tops of the levee turbidites.

Provenance is dominated by igneous rocks yielding 95-100Ma (Cenomanian) detrital zircon ages, consistent with the eastern Peninsular Ranges batholith and related hypabyssal and volcanic rocks. These are some 10 to 15 Myr younger than the rocks of the Alisitos arc that immediately underlies the Rosario Formation (Busby et al. 2006). This suggests that the drainage basin was located largely in the eastern part of Baja California and in what is now Sonora on the Mexican mainland; the upward increasing fraction of mid-Jurassic zircons perhaps indicates a progressive eastward extension of the headwaters of the drainage basin.

The extremely coarse-grained nature of the sediments argues for a steep fluvial system connecting directly to the head of the San Fernando slope channel system on the uppermost slope, consistent with the conclusions of Busby et al. (2002). Given that bedload movement thresholds, slope and discharge are interrelated, it is not possible to make any accurate estimate of the relief of the headwaters, but using the Shields criterion, modest values of 1 m flow depth would be sufficient to mobilize cobbles of 20 cm diameter on a 1° gradient; 100 km stream length (corresponding to the eastern margin of modern Baja California) thus yields headwater elevations of c. 1750 meters. The relative constancy of clast composition through the succession suggests only modest degrees of unroofing, yet the implied degree of erosion and bypass within the slope channel system requires a large total flux towards the basin floor. This argues for a relatively large drainage basin area in order to supply that quantity of sediment. For a river length of 100 km, Hack's Law (Hack 1957) suggests a drainage basin area of the order of 2000 km^2.

The anomalously large boulders of basaltic andesite and limestone originate from the adjacent outcrop belt of the extinct mid-Cretaceous Alisitos arc and associated rudist reefs (Fackler-Adams and Busby 1998), which formed the shoreline to the Rosario basin. Since such boulders cannot have experienced any cross-shelf transport, they were probably derived by wave erosion of sea cliffs immediately adjacent to the head of the canyon that fed the San Fernando channel system. Their transport into deep water was presumably by some high-concentration process. Subaerial debris flows commonly transport boulders of this size, and their reduced immersed weight in a submarine context would facilitate such transport. However, the movement of large heavy objects over long distances by turbidity current-related processes has been described since the earliest acquisition of mooring data (Prior et al. 1987), and these have recently been ascribed to high concentration near-bed sandy layers (Paull et al. 2018). Whatever the specific mechanism (which remains enigmatic), the presence of these boulders indicates that such transport of very coarse material is possible in this setting. It also confirms the direct transfer of material, including fluvially-derived gravels, from the shoreline into deep water. Regardless of whether there was an extensive shelf elsewhere along the coast or not, the feeder canyon to the San Fernando system cut right back to the shoreline.

In summary, the San Fernando system represents a wide range of sedimentological, biological and oceanographic environments. At any one time these varied substantially across the system, largely in response to the variety of current processes and the fluxes of oxygen, organic material and sediment associated with them. The stratification of turbidity currents (and perhaps associated higher density processes) had a particularly profound effect on the distribution of various grain-sizes of sediment across the system.

In addition to these spatial variations, the system evolved through time in a cyclic fashion to generate repeating successions of architecture and facies associations. These temporal variations are largely due to changes in the supply of sediment by gravity flows, almost certainly forced by external factors such as climate-driven changes in run-off and resulting fluvial sediment supply. These may well have been in phase with sea-level fluctuations, though sea-level itself may have had little influence on rates of sediment supply across such a steep margin.

As with so much in the geological record, the preserved deposits are representative of only a fraction the time that the system was active, and only a fraction of the total range of environments that may have been present through time, and thus may not capture all of the processes that were operating. This may be because the evidence is too subtle, its preservation potential is low, or it has been removed by the more energetic processes that represent only a small fraction of the time. For example, there is sparse evidence of the bidirectional currents due to internal tides that are almost universal in modern submarine canyons and slope channels (e.g. Puig et al. 2014 and references therein). Many modern canyon and channel systems host rich and diverse metazoan communities such as the dense benthic communities seen in the coral walls of modern canyons, yet there is little trace of these in San Fernando despite the fact that Gorgonacea and Alcyonacea were both abundant by the late Cretaceous – and by no means all of the taxa in such communities are soft-bodied (Tyler et al., 2009). This may suggest that the stability and relatively soft nature of the substrate in this environment were not suited to the development of such communities, or possibly that such communities are representative only of highstands (and would thus be equivalent to Stage III).

Much—perhaps most of the time that slope channels are active may be not be represented within the surviving deposits due to removal of the thinner-bedded and finer-grained material seen on many modern channel floors, deposited by frequent but less energetic processes (e.g. small turbidity currents and internal tides), (e.g. Hansen 2016), by the less frequent but larger events that dominate the depositional record.

The gross architecture, scale and fill geometry of this system are strikingly similar to those of large-scale slope channel systems of late Miocene/Pliocene age reported in high resolution 2D seismic data from offshore Pakistan (Deptuck et al. 2003) in bathyal water depths, with approximately similar dimensions and proportions of inferred sub-environments to those observed here, though at a very different grain-size. Among slope channel systems of similar calibre, comparable hierarchical approaches have been applied to the description of a number of other examples at outcrop but at strikingly different temporal and stratigraphic scales. What have been described as channel complex sets in the Cretaceous Panoche Formation of the great Valley Group of California (Greene and Surpless 2017) and Nanaimo Group of British Columbia (Bain and Hubbard 2016), while exhibiting broadly similar facies and architectural hierarchy to the San Fernando, are practically an order of magnitude larger. Similarly, conglomeratic channel systems in the Cretaceous Cerro Toro Formation of southern Chile show comparable hierarchical organisation (Beaubouef

2004; Crane and Lowe 2008), but at three or four times the stratigraphic and temporal scale suggested by Sprague et al. (2002, 2005) (Bernhardt et al. 2011, and as applied here to the San Fernando system. All of these systems thus apply the term channel complex set to the scale that we refer to as a channel system. Regardless of the niceties of nomenclature, the implication is that a broadly similar hierarchy of erosionally-bounded stratigraphic elements exists in many coarse-grained slope channel systems, which provides a degree of predictability to architecture and facies distribution both at outcrop and in the subsurface.

ACKNOWLEDGMENTS

Our thanks to Kirt Campion, Tim McHargue and Associate Editor Morgan Sullivan for particularly helpful and constructive reviews. We gratefully acknowledge Luke Fairweather, Alex Fordham, Fabiano Gamberi, Mark McKinnon, Zonia Palacios, Daisy Pataki, Dylan Rood, Sacha Tremblay, Natasha Tuitt, Cristian Vallejo, Hongjie Zhang, and especially Juan Pablo Milana, all of whom helped with the mapping, description and interpretation. Thanks to Claus Fallgatter for help with the drafting of Figure 13. BK and MD sincerely thank Cathy Busby and Bill Morris for introducing us to this system.

REFERENCES

ABREU, V. SULLIVAN, M. PIRMEZ, C. AND MOHRIG, D., 2003, Lateral accretion packages (LAPs): an important reservoir element in deep water sinuous channels: Marine and Petroleum Geology, v. 20, p. 631-648.

ALLEN, J.R.L., 1984, Sedimentary Structures; Their Character and Physical Basis: Amsterdam, Elsevier, Developments in Sedimentology 30, 663 p.

ANDRIEUX, O. COOPER, C.K. AND WOOD, J., 2013, Turbidity Current Measurements in the Congo Canyon: *in* Offshore Technology Conference.

AUDET, D.M., 1998, Mechanical properties of terrigenous muds from levee systems on the Amazon Fan: *in* Stoker, M.S. Evans, D. Cramps, A. eds., Geological Processes on Continental Margins: Sedimentation, Mass-Wasting and Stability: Geological Society of London, Special Publication 129, p. 133-144.

AZPIROZ-ZABALA, M. CARTIGNY, M.J.B. TALLING, P.J. PARSONS, D.R. SUMNER, E.J. CLARE, M.A. SIMMONS, S.M. COOPER, C. AND POPE. E.L., 2017, Newly recognized turbidity current structure can explain prolonged flushing of submarine canyons: Science Advances; v. 3, e1700200

BABONNEAU, N. SAVOYE, B. CREMER, M. AND KLEIN. B, 2002, Morphology and architecture of the present canyon and channel system of the Zaire deep-sea fan: Marine and Petroleum Geology, v. 19, p. 445-467.

BABONNEAU, N. SAVOYE, B. CREMER, M. AND BEZ, M., 2010, Sedimentary architecture in meanders of a submarine channel: detailed study of the present Congo turbidite channel (Zaiango project): Journal of Sedimentary Research, v. 80, p. 852-866.

BAIN, H.A. AND HUBBARD, S.M., 2016, Stratigraphic evolution of a long-lived submarine channel system in the Late Cretaceous Nanaimo Group, British Columbia, Canada: Sedimentary Geology, v. 337, p.113-132.

BAINES, P.G., 1995, Topographic effects in stratified flows. Cambridge Monographs on Mechanics. Cambridge University Press, 482 p.

Barton, M. O'Byrne, C. Pirmez, C. Prather, B. Van der Vlugt, F. Alpak, F.O. and Sylvester, Z., 2010, Turbidite channel architecture: Recognizing and quantifying the distribution of channel-base drapes using core and dipmeter data: in Dipmeter and Borehole Image Log Technology, AAPG Memoir 92, American Association of Petroleum Geologists, Poppelreiter, M., Garcia-Carballido, C and Kraaijveld, M, eds. p.195-210.

Beaubouef, R.T., 2004, Deep-water leveed-channel complexes of the Cerro Toro Formation, Upper Cretaceous, southern Chile: AAPG Bulletin, v. 88, p. 1471-1500.

Birman, V.K. Meiburg, E. and Kneller, B., 2009, The shape of submarine levees: exponential or power law?: Journal of Fluid Mechanics, v. 619, p. 367–376.

Bridge, J.S., 2006, Fluvial facies models: recent developments: SEPM Special Publication 84, 85 p.

Bernhardt, A., Jobe, Z.R. and Lowe, D.R., 2011, Stratigraphic evolution of a submarine channel–lobe complex system in a narrow fairway within the Magallanes foreland basin, Cerro Toro Formation, southern Chile: Marine and Petroleum Geology, v. 28, p.785-806.

Busby, C. Smith, D. Morris, W. and Fackler-Adams, B., 1998, Evolutionary model for convergent margins facing large ocean basins: Mesozoic Baja California, Mexico: Geology, v. 26, p. 227-230.

Busby, C.J. Yip, G. Blikra, L. and Renne, P., 2002, Coastal landsliding and catastrophic sedimentation triggered by Cretaceous-Tertiary bolide impact: A Pacific margin example?: Geology, v. 30, p. 687-690.

Busby, C. Fackler Adams, B. Mattinson, J. and Deoreo, S., 2006, View of an intact oceanic arc, from surficial to mesozonal levels: Cretaceous Alisitos arc, Baja California: Journal of Volcanology and Geothermal Research, v. 149, p. 1– 46.

Camacho, H. Busby, C.J. and Kneller, B., 2002, A new depositional model for the classical turbidite locality at San Clemente State Beach, California: AAPG Bulletin, v. 86, p. 1543-1560.

Callow, R.H. McIlroy, D., Kneller, B. and Dykstra, M., 2013, Integrated ichnological and sedimentological analysis of a Late Cretaceous submarine channel-levee system: The Rosario Formation, Baja California, Mexico: Marine and Petroleum Geology, v. 41, p. 277-294.

Campion, K.M. Sprague, A.R. Mohrig, D. Lovell, R.W. Drzewiecki, P.A. Sullivan, M.D. Ardill, J.A. Jensen, G.N. and Sickafoose, D.K., 2003, Outcrop expression of confined channel complexes. *In* Gulf Coast Section SEPM, Deep Water Reservoirs of the World. p. 127-151.

Clark, J.D., Kenyon, N.H. and Pickering, K.T. 1992, Quantitative analysis of the geometry of submarine channels: implications for the classification of submarine fans: Geology, v. 20, p. 633-636.

Crane, W.H. and Lowe, D.R., 2008, Architecture and evolution of the Paine channel complex, Cerro Toro formation (Upper Cretaceous), Silla syncline, Magallanes basin, Chile: Sedimentology, v. 55, p. 979-1009.

Dalla Valle, G. and Gamberi, F., 2011, Slope channel formation, evolution and backfilling in a wide shelf, passive continental margin (Northeastern Sardinia slope, Central Tyrrhenian Sea): Marine Geology, v. 286, p. 95-105.

DAMUTH, J.E., FLOOD, R.D., PIRMEZ, C. AND MANLEY, P.L., 1995, Architectural elements and depositional processes of Amazon deep-sea fan imaged by long-range sidescan sonar (GLORIA), bathymetric swath-mapping (Sea Beam), high-resolution seismic and piston-core data. In Atlas of Deep Water Environments, Springer, Dordrecht, p. 105-121.

DASTAS, N., CHAMBERLAIN, J. AND GARB, M., 2014, Cretaceous-Paleogene dinoflagellate biostratigraphy and the age of the Clayton Formation, southeastern Missouri, USA.:Geosciences, v. 4, p.1-29.

DIETRICH, W.E. AND WHITING, P., 1989, Boundary shear stress and sediment transport in river meanders of sand and gravel: River meandering, v. 12, p. 1-50.

DEPTUCK, M.E. STEFFENS, G.S. BARTON, M. AND PIRMEZ, C., 2003, Architecture and evolution of upper fan channel-belts on the Niger Delta slope and in the Arabian Sea: Marine and Petroleum Geology, v. 20, p. 649-676.

DEPTUCK, M.E. SYLVESTER, Z. PIRMEZ, C. AND O'BYRNE, C., 2007, Migration–aggradation history and 3-D seismic geomorphology of submarine channels in the Pleistocene Benin-major Canyon, western Niger Delta slope: Marine and Petroleum Geology, v. 24, p. 406-433.

DEVRIES, M.B. AND LINDHOLM, R.M., 1994, December. Internal architecture of a channel-levee complex, Cerro Toro Formation, southern Chile: *In* Submarine fans and turbidite systems: Gulf Coast Section SEPM 15th Annual Research Conference, p. 105-114.

DICKINSON, W.R., 1985, Interpreting provenance relations from detrital modes of sandstones: *in* Zuffa, G.G., ed., Provenance of Arenites. Springer Netherlands, Dordrecht, p. 333–361.

Droz, L. Marsset, T. Ondras, H. Lopez, M. Savoye, B. and Spy-Anderson, F.L., 2003, Architecture of an active mud-rich turbidite system: The Zaire Fan (Congo–Angola margin southeast Atlantic: Results from ZaiAngo 1 and 2 cruises: AAPG Bulletin, v. 87, p. 1145-1168.

Dykstra, M. and Kneller, B., 2007, Canyon San Fernando, Baja California, Mexico: A Deep-marine channel-levee complex that evolved from submarine canyon confinement to unconfined deposition: *in* T. H. Nilsen, R. D. Shew, G. S. Steffens, and J. R. J. Studlick, eds., Atlas of deep-water outcrops: AAPG Studies in Geology 56, CD-ROM, 14 p.

Dykstra, M. and Kneller, B., 2009, Lateral accretion in a deep-marine channel complex: implications for channellized flow processes in turbidity currents: Sedimentology, v. 56, p. 1411-1432.

Fackler-Adams, B.N. and Busby, C.J., 1998, Structural and stratigraphic evolution of extensional oceanic arcs: Geology, v. 6, p. 735–738

Fildani, A. Hubbard, S.M. Covault, J.A. Maier, K.L. Romans, B.W. Traer, M. and Rowland, J.C., 2013, Erosion at inception of deep-sea channels: Marine and Petroleum Geology, v. 41, p. 48-61.

Firth, J.V., 1987, Dinoflagellate biostratigraphy of the Maastrichtian to Danian interval in the US Geological Survey Albany core, Georgia, USA: Palynology, v. 11, p. 199-216.

Firth, J.V., 1993. Dinoflagellate assemblages and sea-level fluctuations in the Maastrichtian of southwest Georgia: Review of Palaeobotany and Palynology, v. 79, p.179-204.

Gamberi, F. and Marani, M., 2011, Geomorphology and sedimentary processes of a modern confined braided submarine channel belt (Stromboli Slope Valley, southeastern Tyrrhenian Sea): Journal of Sedimentary Research, v. 81, p. 686–701.

Gamberi, F. Rovere, M. and Marani, M., 2011, Mass-transport complex evolution in a tectonically active margin (Gioia Basin, Southeastern Tyrrhenian Sea): Marine Geology, v. 279, p. 98-110.

Gamberi, F. Rovere, M. Dykstra, M. Kane, I.A. and Kneller, B.C., 2013, Integrating modern seafloor and outcrop data in the analysis of slope channel architecture and fill: Marine and Petroleum Geology, v. 41, p. 83-103.

García, M.H., 1994, Depositional turbidity currents laden with poorly sorted sediment: Journal of Hydraulic Engineering, v. 120, p. 1240-1263.

García, M. and Parker, G., 1991, Entrainment of bed sediment into suspension: Journal of Hydraulic Engineering, v. 117, p. 414-435.

García, M. and Parker, G., 1993, Experiments on the entrainment of sediment into suspension by a dense bottom current: Journal of Geophysical Research-All Series, v. 98, p. 4793-4793.

Gastil, R.G. Krummenacher, D. Doupont, J. and Bushes, J., 1974, The batholith belt of southern California and western Mexico: Pacific Geology, v. 8, p. 73-78.

Gastil, R.G. Kimbrough, D.L. Kimbrough, J.M. Grove, M. and Shimizu, M., 2014, The Sierra San Pedro Mártir zoned pluton, Baja California, Mexico: In Morton, D.M. and Miller, F.K., eds, Peninsular Ranges Batholith, Baja California and Southern California. Geological Society of America Memoir 211, p. 739-758.

Greene, T.J. and Surpless, K.D., 2017, Facies architecture and provenance of a boulder-conglomerate submarine channel system, Panoche Formation, Great Valley

Group: A forearc basin response to middle Cretaceous tectonism in the California convergent margin: Geosphere, v. 13, p. 838-869.

HACK, J.T., 1957, Studies of longitudinal profiles in Virginia and Maryland: U.S. Geological Survey Professional Paper 294-B, 52 p.

HANSEN, L. A. S., 2016, Reservoir prediction in channel related thin-bedded turbidites: Ph.D. thesis, University of Aberdeen, Aberdeen, United Kingdom

HANSEN, L.A. CALLOW, R.H. KANE, I.A. GAMBERI, F. ROVERE, M. CRONIN, B.T. AND KNELLER, B.C., 2015, Genesis and character of thin-bedded turbidites associated with submarine channels: Marine and Petroleum Geology, v. 67, p. 852-879.

HANSEN, L, CALLOW, R. KANE, I. AND KNELLER, B., 2017a, Differentiating submarine channel related thin-bedded turbidite facies: Outcrop example from the Rosario Formation, Mexico: Sedimentary Geology, v. 358, p. 19-34.

HANSEN, L. JANOCKO, M. KANE, I AND KNELLER, B., 2017b, Submarine channel evolution, terrace development, and preservation of intra-channel thin-bedded turbidites: Mahin and Avon channels, offshore Nigeria: Marine Geology, v. 383, p. 146–167.

HEIN, F.J. AND WALKER, R.G., 1982, The Cambro-Ordovician Cap Enragé Formation, Queébec, Canada: conglomeratic deposits of a braided submarine channel with terraces: Sedimentology, v. 29, p. 309-352.

HELENES, J., 1984. Dinoflagellates from Cretaceous to Early Tertiary rocks of the Sebastian Vizcaino Basin, Baja California, Mexico.

HELENES, J. AND TÉLLEZ-DUARTE, M.A., Paleontological evidence of the Campanian to Early Paleocene paleogeography of Baja California; Palaeogeography, Palaeoclimatology, Palaeoecology, v. 186, p.61-80.

Hiscott, R.N. Hall, F.R. and Pirmez, C., 1997, Turbidity-current overspill from the Amazon Channel: texture of the silt/sand load, paleoflow from anisotropy of magnetic susceptibility, and implications for flow processes: *in* Proceedings-Ocean Drilling Program Scientific Results, p. 53-78. National Science Foundation.

Hodgson, D.M. Flint, S.S. Hodgetts, D. Drinkwater, N.J. Johannessen, E.P. and Luthi, S.M., 2006. Stratigraphic evolution of fine-grained submarine fan systems, Tanqua depocenter, Karoo Basin, South Africa: Journal of Sedimentary Research, v. 76, p. 20-40.

Hodgson, D.M. Kane, I.A. Flint, S.S. Brunt, R.L. and Ortiz-Karpf, A., 2016, Time-transgressive confinement on the slope and the progradation of basin-floor fans: Implications for the sequence stratigraphy of deep-water deposits: Journal of Sedimentary Research, v. 86, p. 73-86.

Hubbard, S.M. Covault, J.A. Fildani, A. and Romans, B.W., 2014, Sediment transfer and deposition in slope channels: deciphering the record of enigmatic deep-sea processes from outcrop: Geological Society of America Bulletin, v. 126, p. 857-871.

Hubbard, S.M. and Schultz, M.R., 2008. Deep burrows in submarine fan-channel deposits of the Cerro Toro Formation (Cretaceous), Chilean Patagonia: implications for firmground development and colonization in the deep sea: Palaios, v. 23, p.223-232.

Hübscher, C. Spiess, V. Breitzke, M. and Weber, M.E., 1997, The youngest channel-levee system of the Bengal Fan: Results from digital sediment echosounder data: Marine Geology, v. 141, p. 125-145.

Hughes-Clarke, J.E. Shor, A.N. Piper, D.J. and Mayer, L.A., 1990, Large-scale current-induced erosion and deposition in the path of the 1929 Grand Banks turbidity current: Sedimentology, v. 37, p. 613-629.

Ito, M., 2019. Lithofacies architecture of gravel-wave deposits: Insights into the origins of coarse-grained gravity-flow deposits: Sedimentary Geology, v. 82, p.36-46.

Janocko, M. Nemec, W. Henriksen, S. and Warchoł, M., 2013, The diversity of deep-water sinuous channel belts and slope valley-fill complexes: Marine and Petroleum Geology, v. 41, p. 7-34.

Johnson, S.D. Flint, S. Hinds, D. and De Ville Wickens, H., 2001, Anatomy, geometry and sequence stratigraphy of basin floor to slope turbidite systems, Tanqua Karoo, South Africa: Sedimentology, v. 48, p. 987-1023.

Kane, I.A. Kneller, B.C. Dykstra, M. Kassem, A. and McCaffrey, W.D., 2007, Anatomy of a submarine channel–levee: an example from Upper Cretaceous slope sediments, Rosario Formation, Baja California, Mexico: Marine and Petroleum Geology, v. 24, p. 540-563.

Kane, I.A. Dykstra, M.L. Kneller, B.C. Tremblay, S. and McCaffrey, W.D., 2009, Architecture of a coarse-grained channel–levée system: the Rosario Formation, Baja California, Mexico: Sedimentology, v. 56, p. 2207-2234.

Kane, I.A. and Hodgson, D.M., 2011, Sedimentological criteria to differentiate submarine channel levee subenvironments: exhumed examples from the Rosario Fm.(Upper Cretaceous) of Baja California, Mexico, and the Fort Brown Fm.(Permian), Karoo basin, S. Africa: Marine and Petroleum Geology, 28, p. 807-823.

Khripounoff, A. Crassous, P. Bue, N.L. Dennielou, B. and Jacinto, R.S., 2012, Different types of sediment gravity flows detected in the Var submarine canyon (northwestern Mediterranean Sea): Progress in Oceanography, v. 106, p. 138-153.

Kidd, R.B. Lucchi, R.G. Gee, M. and Woodside, J.M., 1998. Sedimentary processes in the Stromboli Canyon and Marsili Basin, SE Tyrrhenian Sea: results from side-scan sonar surveys: Geo-Marine Letters, v. 18, p. 146–154.

Kneller, B., 2003, The influence of flow parameters on turbidite slope channel architecture: Marine and Petroleum Geology, v. 206, p. 901-910.

Kneller, B. and Buckee, C., 2000, The structure and fluid mechanics of turbidity currents: a review of some recent studies and their geological implications: Sedimentology, v. 47, p. 62-94.

Kolla, V. Bandyopadhyay, A. Gupta, P. Mukherjee, B. and Ramana, D.V., 2012, Morphology and internal structure of a recent upper Bengal Fan-valley complex. In Application of the Principles of Seismic Geomorphology to Continental-Slope and Base-of-Slope Systems: Case Studies from Seafloor and Near-Seafloor Analogues: SEPM Special Publication No. 99. p. 347–369.

Kolla, V. and Coumes, F., 1987, Morphology, internal structure, seismic stratigraphy, and sedimentation of Indus Fan: AAPG Bulletin, v. 71, p. 650-677.

Konsoer, K. Zinger, J. and Parker, G., 2013, Bankfull hydraulic geometry of submarine channels created by turbidity currents: Relations between bankfull channel characteristics and formative flow discharge: Journal of Geophysical Research: Earth Surface. V. 118, p. 216–228.

Li, P., 2017, Architecture and sedimentology of multiscale slope channel fills: insights from the analogues in outcrop and subsurface. Ph.D. thesis, University of Aberdeen, Aberdeen, United Kingdom.

Li P., Kneller, B. ,Thompson P., Bozetti G. and Santos T.D., 2018, Architectural and facies organisation of slope channel fills: Upper Cretaceous Rosario Formation, Baja California, Mexico: Marine and Petroleum Geology, v. 92, p. 632-649.

Lipman, P.W., 1992, Magmatism in the Cordilleran United States; progress and problems: The Geology of North America, v. 3, p. 481-514.

Lucas-Clark, J., 2006, Small peridinioid dinoflagellate cysts from the Paleocene of South Carolina, USA: Palynology, v. 30, p.183-210.

Lunt, I.A. and Bridge, J.S., 2004, Evolution and deposits of a gravelly braid bar, Sagavanirktok River, Alaska: Sedimentology, v. 51, p. 415-432.

Maier, K.L. Fildani, A. McHargue, T.R. Paull, C.K. Graham, S.A. and Caress, D.W., 2012, Punctuated Deep-Water Channel Migration: High-Resolution Subsurface Data from the Lucia Chica Channel System, Offshore California, USA: Journal of Sedimentary Research, v. 82, p. 1-8.

Maier, K.L. Fildani, A. Paull, C.K. McHargue, T.R. Graham, S.A. and Caress, D.W., 2013, Deep-sea channel evolution and stratigraphic architecture from inception to abandonment from high-resolution Autonomous Underwater Vehicle surveys offshore central California: Sedimentology, v. 60, p. 935-960.

Malinverno, A. Ryan, W.B. Auffret, G. and Pautot, G., 1988, Sonar images of the path of recent failure events on the continental margin off Nice, France: Geological Society of America Special Papers, v. 229, p. 59-76.

MACAULEY, R.V. AND HUBBARD, S.M., 2013, Slope channel sedimentary processes and stratigraphic stacking, Cretaceous Tres Pasos Formation slope system, Chilean Patagonia: Marine and Petroleum Geology, v. 41, p. 146–162.

MAYALL, M. AND STEWART, I., 2000, December. The architecture of turbidite slope channels: *in* Deep-Water Reservoirs of the World: SEPM, Gulf Coast Section 20th Annual Research Conference, v. 578, p. 586.

MAYALL, M. JONES, E. AND CASEY, M., 2006, Turbidite channel reservoirs—Key elements in facies prediction and effective development: Marine and Petroleum Geology, v. 23, p. 821-841.

MCARTHUR, A.D. KNELLER, B.C. SOUZA, P.A. KUCHLE, J., 2016, Characterization of deep-marine channel-levee complex architecture with palynofacies: an outcrop example from the Rosario Formation, Baja California, Mexico: Marine and Petroleum Geology, v. 73, p. 157–173

MCARTHUR, A.D. KANE, I., BOZETTI, G., HANSEN, L, AND KNELLER, B., 2019, Supercritical flows over-spilling from bypass-dominated submarine channels and the development of overbank bedforms: The Depositional Record.

MCDOWELL, F.W. ROLDÁN-QUINTANA, J. AND CONNELLY, J.N., 2001, Duration of Late Cretaceous–early Tertiary magmatism in east-central Sonora, Mexico: Geological Society of America Bulletin, v. 113, p. 521-531.

MCHARGUE, T. PYRCZ, M.J. SULLIVAN, M.D. CLARK, J.D. FILDANI, A. ROMANS, B.W. COVAULT, J.A. LEVY, M. POSAMENTIER, H.W. AND DRINKWATER, N.J., 2011, Architecture of turbidite channel systems on the continental slope: patterns and predictions: Marine and Petroleum Geology, v. 28, p. 728-743.

Miall, A.D., 1977, A review of the braided-river depositional environment: Earth-Science Reviews, v. 13, p. 1-62.

Miall, A., 2013, The geology of fluvial deposits: sedimentary facies, basin analysis, and petroleum geology. Springer.

Middleton, G.V. and Southard, J.B., 1984, Mechanics of sediment movement: SEPM Short Course Notes.

Migeon, S. Savoye, B. and Faugeres, J.C., 2000, Quaternary development of migrating sediment waves in the Var deep-sea fan: distribution, growth pattern, and implication for levee evolution: Sedimentary Geology, v. 133, p. 265-293.

Migeon, S. Mulder, T. Savoye, B. and Sage, F., 2006, The Var turbidite system (Ligurian Sea, northwestern Mediterranean)—morphology, sediment supply, construction of turbidite levee and sediment waves: implications for hydrocarbon reservoirs: Geo-Marine Letters, v. 26, p. 361-371.

Migeon, S. Mulder, T. Savoye, B. and Sage, F., 2012, Hydrodynamic processes, velocity structure and stratification in natural turbidity currents: results inferred from field data in the Var Turbidite System: Sedimentary Geology, v. 245, p. 48-62.

Miller, M.C. McCave, I.N. and Komar, P.D., 1977, Threshold of sediment motion under uinidirectional currents: Sedimentology, v. 24, p. 507-527.

Morris, S.A. Kenyon, N.H. Limonov, A.F. And Alexander, J., 1998, Downstream changes of large-scale bedforms in turbidites around the Valencia channel mouth, north-west Mediterranean: implications for palaeoflow reconstruction: Sedimentology, v. 45, p. 365–377.

Morris, W. R., 1992, The depositional framework, paleogeography and tectonic development of the Late Cretaceous through Paleocene Peninsular Range forearc basin in the Rosario Embayment, Baja California, Mexico: Ph.D. thesis, University of California, Santa Barbara, 240 p.

Morris, W. and Busby-Spera, C., 1990, A submarine-fan valley-levee complex in the Upper Cretaceous Rosario Formation: Implication for turbidite facies models: Geological Society of America Bulletin, v. 102, p. 900-914.

Mutti, E. and Ricci Lucchi, F., 1972, Le torbiditi dell'Appennino settentrionale: introduzione all'analisi di facies. Memorie della Societa Geologica Italiana, v. 11, p. 161-199.

Nakajima, T. Peakall, J. McCaffrey, W.D. Paton, D.A. and Thompson, P.J., 2009, Outer-bank bars: a new intra-channel architectural element within sinuous submarine slope channels: Journal of Sedimentary Research, v. 79, p. 872-886.

Nakajima, T. and Kneller, B., 2013, Quantitative analysis of the geometry of submarine levees: Sedimentology, v. 60, p. 877–910.

Normark, W.R. Piper, D.J.W. And Hess, G.R., 1979, Distributary channels, sand lobes, and meso-topography of Navy Submarine Fan, California Borderland, with applications to ancient fan sediments: Sedimentology, v. 26, p. 749–774.

Oskin, M. and Stock, J., 2003, Pacific–North America plate motion and opening of the Upper Delfín basin, northern Gulf of California, Mexico: Geological Society of America Bulletin, v. 115, p. 1173-1190.

Paull, C.K. Ussler III, W. Caress, D.W. Lundsten, E. Covault, J.A. Maier, K.L. Xu, J. and Augenstein, S., 2010, Origins of large crescent-shaped bedforms within the axial channel of Monterey Canyon, offshore California: Geosphere, v. 6, p. 755-774.

PAULL, C.K, and 21 others, 2018, Powerful turbidity currents driven by dense basal layers: Nature Communications, DOI: 10.1038/s41467-018-06254-6

PEAKALL, J. MCCAFFREY, B. AND KNELLER, B., 2000, A process model for the evolution, morphology, and architecture of sinuous submarine channels: Journal of Sedimentary Research, v. 70, p. 434-448.

PEAKALL, J. KANE, I.A. MASSON, D.G. KEEVIL, G. MCCAFFREY, W. AND CORNEY, R., 2012, Global (latitudinal) variation in submarine channel sinuosity: Geology, v. 40, p. 11-14.

PIPER, D.J. AND KONTOPOULOS, N., 1994, Bedforms in submarine channels: comparison of ancient examples from Greece with studies of Recent turbidite systems: Journal of Sedimentary Research, v. 64, p. 247-252

PIPER, D.J. AND SAVOYE, B., 1993, Processes of late Quaternary turbidity current flow and deposition on the Var deep-sea fan, north-west Mediterranean Sea: Sedimentology, v. 40, p. 557-582.

PIPER, D.J. AND SAVOYE, B., 1993. Processes of Late Quaternary turbidity current flow and deposition on the Var deep sea fan, north-west Mediterranean Sea: Sedimentology, v. 40, p. 557-582.

PIPER, D.J. SHOR, A.N. AND HUGHES CLARKE, J.E.H., 1988, The 1929 “Grand Banks” earthquake, slump, and turbidity current: Geological Society of America Special Papers, v. 229, p. 77-92.

PIRMEZ, C. HISCOTT, R.N. AND KRONEN, J.D., 1997, Sandy turbidite successions at the base of channel-levee systems of the Amazon Fan revealed by FMS logs and cores: unraveling the facies architecture of large submarine fans: *in* Proceedings of the Ocean Drilling Program. Scientific results, v. 155, p. 7-33. Ocean Drilling Program.

Pirmez, C. Beaubouef, R.T. Friedmann, S.J. And Mohrig, D.C., 2000, Equilibrium profiles and base level in submarine channel: examples from late Pleistocene systems and implications for the architecture of deepwater reservoirs, in Weimer, P., Slatt, R.M., Coleman, J., Rosen, N.C., Nelson, H., Bouma, A.H., Styzen, M.J., and Lawrence, D.T., eds., Deep-Water Reservoirs of the World: SEPM, Gulf Coast Section, 20th Annual Research Conference, p. 782–805.

Posamentier, H.W., 2003, Depositional elements associated with a basin floor channel-levee system: case study from the Gulf of Mexico: Marine and Petroleum Geology, v. 20, p. 677-690.

Posamentier, H.W. And Walker, R.G., 2006, Deep-water turbidites and submarine fans, in Posamentier, H.W., and Walker, R.G., eds., Facies Models Revisited: SEPM, Special Publication 84, p. 397-520.

Prelat, A. Covault, J.A. Hodgson, D.M. Fildani, A. and Flint, S.S., 2010, Intrinsic controls on the range of volumes, morphologies, and dimensions of submarine lobes: Sedimentary Geology, v. 232, p. 66-76.

Prior, D.B. Bornhold, B.D. Wiseman, W.J. and Lowe, D.R., 1987, Turbidity current activity in a British Columbia fjord: Science, v. 237, p. 1330-1333.

Sawyer, D.E. Flemings, P.B. Shipp, R.C. and Winker, C.D., 2007, Seismic geomorphology, lithology, and evolution of the late Pleistocene Mars-Ursa turbidite region, Mississippi Canyon area, northern Gulf of Mexico: AAPG Bulletin, v. 91, p. 215-234.

Puig, P., Palanques,, A. and Martín,, J., 2014. Contemporary sediment-transport processes in submarine canyons: Annual Review of Marine Science, 6, p. 53-77

Sequeiros, O. E., Spinewine, B., Beaubouef, R. T., Sun, T., García, M. H. and Parker, G., 2010, Characteristics of velocity and excess density profiles of saline underflows and turbidity currents flowing over a mobile bed: Journal of Hydraulic Engineering, v. 136, p. 412–433.

Shor, A.N. Piper, D.J. Clarke, J.E.H. and Mayer, L.A., 1990, Giant flute-like scour and other erosional features formed by the 1929 Grand Banks turbidity current: Sedimentology, v. 37, p. 631-645.

Sharman, G.R. Graham, S.A. Grove, M. Kimbrough, D.L. and Wright, J.E., 2015, Detrital zircon provenance of the Late Cretaceous–Eocene California forearc: Influence of Laramide low-angle subduction on sediment dispersal and paleogeography: Geological Society of America Bulletin, v. 127, p. 38-60.

Shields, A., 1936, Anwendung der Ähnlichkeitsmechanik auf die Geschiebebewegung: Berlin, Preussische Versuchanstalt für Wasserbau und Schiffbau, Mitteilungen, no. 26, 25 p.

Sikkema, W. and Wojcik, K.M., 2000, December. 3D visualization of turbidite systems, Lower Congo Basin, offshore Angola: *in* Deep-Water Reservoirs of the World, SEPM, Gulf Coast Section 20th Annual Research Conference, p. 928-939.

Sprague, A.R. Sullivan, M.D. Campion, K.M. Jensen, G.N. Goulding, D.K. Sickafoose, D.K. and Jennette, D.C., 2002, The physical stratigraphy of deep-water strata: a hierarchical approach to the analysis of genetically related elements for improved reservoir prediction: American Association of Petroleum Geologists Annual Meeting abstracts, Houston, Texas, p. 10-13.

Sprague, A.R.G. Garfield, T.R. Goulding, F.J. Beaubouef, R.T. Sullivan, M.D. Rossen, C. Campion, K.M. Sickafoose, D.K. Abreu, V. Schellpeper, M.E. and

Jensen, G.N., 2005, Integrated slope channel depositional models: the key to successful prediction of reservoir presence and quality in offshore West Africa: CIPM, cuarto E-Exitep, p.1-13.

Stevenson, C.J. Jackson, C.A.L. Hodgson, D.M. Hubbard, S.M. and Eggenhuisen, J.T., 2015, Deep-water sediment bypass: Journal of Sedimentary Research, v. 85, p. 1058-1081.

Stevenson, C.J. Talling, P.J. Wynn, R.B. Masson, D.G. Hunt, J.E. Frenz, M. Akhmetzhanhov, A. and Cronin, B.T., 2013, The flows that left no trace: Very large-volume turbidity currents that bypassed sediment through submarine channels without eroding the sea floor: Marine and Petroleum Geology, v. 41, p. 186-205.

Stow, D.A.V. Hernández-Molina, F.J. Llave, E. Bruno, M. García, M. del Rio, V.D. Somoza, L. and Brackenridge, R.E., 2013, The Cadiz Contourite Channel: Sandy contourites, bedforms and dynamic current interaction: Marine Geology, v. 343, p. 99-114.

Szuman, M., 2009, Forward seismic modelling and spectral decomposition of deepwater slope deposits in outcrop and subsurface. Ph.D. thesis, University of Aberdeen, Aberdeen, United Kingdom.

Thompson, P. J-P., 2010, The Spatial and Temporal Variation of Stratigraphic Elements within the San Fernando Channel System, Baja California, Mexico. Ph.D. thesis, University of Aberdeen, Aberdeen, United Kingdom.

Tuitt, N., 2015, 4D Interpretation of Texture and Architecture of a Coarse Grained Slope Channel System Using Automated Statistics From High Resolution Outcrop Photography. Ph.D. thesis, University of Aberdeen, Aberdeen, United Kingdom.

Tyler, P., Amaro, T., Arzola, R., Cunha, M.R., de Stigter, H., Gooday, A., Huvenne, V., Ingels, J., Kiriakoulakis, K., Lastras, G. and Masson, D., 2009. Europe's Grand Canyon, Nazare submarine canyon: Oceanography, v. 22, p. 46-57.

Van Rijn, L.C., 1993, Principles of sediment transport in rivers, estuaries and coastal seas: Amsterdam, Aqua publications.

Viana, A. Figueiredo, A. Faugres, J.C. Lima, A. Gonthier, E. Brehme, I. and Zaragosi, S., 2003, The Sao Tome deep-sea turbidite system (southern Brazil Basin): Cenozoic seismic stratigraphy and sedimentary processes: AAPG bulletin, v. 87, p. 873-894.

Wang. Z., 2018, High-concentration basal layers in oceanic turbidity currents: 9th International Conference on Asian Marine Geology, abstracts.

Williams, T.A. and Graham, S.A., 2013, Controls on forearc basin architecture from seismic and sequence stratigraphy of the Upper Cretaceous Great Valley Group, central Sacramento Basin, California: International Geology Review, 55, p. 2030-2059.

Wynn, R.B. and Stow, D.A., 2002, Classification and characterisation of deep-water sediment waves: Marine Geology v. 192, p. 7-22.

Xu, J.P. Barry, J.P. and Paull, C.K., 2013, Small-scale turbidity currents in a big submarine canyon: Geology, v. 41, p. 143–146, doi: 10.1130 /G33727.1.

Zhang, H., 2013, Spectral decomposition of outcrop-based synthetic seismic data, applied to reservoir prediction in deep-water settings. Ph.D. thesis, University of Aberdeen, Aberdeen, United Kingdom

FIGURES

Figure 1. (A) Regional geology and location map, showing the distribution of mid-Cretaceous arc and late Cretaceous to Paleogene fore-arc rocks. Study area indicated by red box (B) Geological Map of the Rosario Embayment of the Peninsular Ranges Forearc Basin Complex, with study area outlined. (C) Stratigraphic column of the Rosario embayment, summarizing local litho- and chronostratigraphy.

Figure 2. (A) Geological map of the Arroyo San Fernando area, with geology overlaid on satellite images, showing channel complex set boundaries (dotted where inferred. Dominant lithologies shown, where they can be mapped: brown – mainly conglomerate; yellow – mainly sandstone; blue – debrite; green – mainly thin-bedded heterolithic sediments; grey – mainly hemipelagic mudstone. Dots and letters show locations shown of sections where levee grain-size samples were taken. Pooled paleocurrent data for the channel belt, terraces and levee shown in the rose diagrams. (B) enlargement of boxed area in A, showing channel complex set boundaries and dominant lithologies. Also shown (purple lines) are locations of logs used for vertical sequence analysis.

Figure 3. (A) Simplified composite depositional strike section of Arroyo San Fernando channel system, approximately to scale, showing the main channel system boundary, channel complex set boundaries, distribution of architectural components: channel belt, with axial region, off-axis, channel belt margin, and channel belt boundary zone; external levee with inner and outer regions separated by the levee

crest. (B) Form of the south-eastern boundary of the channel system cutting the slope sediments, using pseudowells based on outcrop configuration; surface constructed in Petrel®. (C) Schema of hierarchy of surfaces and stage boundaries.

Figure 4. (A) Panorama of axial region of Arroyo San Fernando channel system showing CCS B, C and D (channel complex set boundaries in red; channel complex boundaries in CCS-C Stage II in yellow. (B) Panorama of upper part of CCS-A Stage I, with continuous sandstone, cut by base of Stage I of CCS-B, showing location of log in Figure 4C. (C) representative log of lower part of Stage I (CCS-B) (from Li et al., 2018). Note that it is difficult to differentiate the CCS boundary in 4B since CCS-B Stage I cuts right into CCS-A Stage I.

Figure 5. vertical facies transition analysis for: (A) all of CCS-B; (B) CCS-B Stage I; (C) CCS-B Stage II, axial; (D) CCS-B Stage II marginal. Each showing: composite stratigraphic successions; facies frequency distributions (including erosional surfaces with relief > 20 cm); and facies relationship diagram, showing the preferred vertical facies transitions. Facies: F1, mudstone; F2, thin-bedded mudstone and sandstone; F3, sandstone (a, structured sandstone; b, structureless; c, pebbly); F4, conglomerate (a, disorganized granules-pebbles; b, organized granules-pebbles; c, disorganized pebbles-cobbles; d, organized pebbles-cobbles); F5, pebbly mudstone of mud-matrix rich conglomerate; Es, erosion surfaces. Modified from Li et al. (2018).

Figure 6. Photographs of representative facies. (A) Coarse-grained bars from CCS-A Stage I. (B) Enlarged image of area shown in upper rectangle in A, showing boulder-

grade, well-sorted open-framework bar core. (C) Enlarged image of area shown in lower rectangle in A, showing variations in texture, grain-size and sorting of disorganized conglomerate within a single bar; uppermost gravel possibly constitutes an armored layer; isolated coarse sandstone lenses are presumed erosional remnants. (D) Cross-stratified gravel, indicating migrating bedform or accreting bar; direction of accretion is approximately transverse to channel. (E) *a*-parallel imbrication fabric in moderately to well-sorted small cobble grade conglomerate of Stage II. (F) Graded, well-sorted, imbricated conglomerate suggesting deposition by a single event. 1.5 cm coin for scale. (G) Massive to weakly stratified coarse to very coarse sandstone of uppermost Stage I (CCS-A) cut by basal erosion surface of succeeding channel complex set. (H) Very coarse grained sandstone of Stage I containing rafted block of very thin bedded siltstone and mudstone. (I) Pebbly mudstone (debrite). (J) Terrace; medium-bedded graded very coarse/granule grade sandstone-to-mudstone couplets with climbing ripples. (K) Thin to medium bedded sandstone- mudstone couplets of proximal external levee. (L) Very thin bedded sandstone-mudstone couplets of distal external levee (from McArthur et al. 2016).

Figure 7. Photomosaic (A) and line drawing (B) of representative portion of Stage I (CCS-A), showing characteristic lateral impersistence of facies; isolated coarse sandstone lenses are presumed erosional remnants except for a single more continuous sandstone that marks a channel complex boundary; base of overlying channel complex denoted by heavy line (from Thompson 2010). S1; Massive, normally graded, moderately sorted sandstone. S2; Massive, normally-graded, poorly sorted sandstone. S3; Massive, ungraded, moderately sorted sandstone. Cg1; sand/mud matrix supported conglomerate. Cg2; pebbly mudstone. Cg11; sandy matrix

supported conglomerate. Cg10; massive, clast supported conglomerate. Cg12; massive, ungraded, moderately sorted conglomerate. Cg3; other poorly to well sorted conglomerate. Cg4; normally graded conglomerate. Cg5; normally graded, imbricated conglomerate. Cg7; inverse to normally graded ,moderately sorted conglomerate. Cg8; normally graded, well sorted conglomerate. (C) Photograph illustrating typical facies variability and lack of continuity; middle of image shows a bar draped with sand, both of which are truncated by an erosion surface.

Figure 8. (A) Photomosaic showing essentially tabular nature of the conglomerate bodies forming the Stage II channel complexes (CCS-B in this case). (B) and line drawing detail of area outlined in (A) illustrating internal (lateral accretion) architecture of the coarse-grained component of Stage II channel complexes (from Li et al., 2018; see also Thompson 2010). (C) Representative logs and correlation of Stage II (CCS-B) (from Li et al. 2018).

Figure 9. Representative logs of different thin-bed environments associated with the San Fernando channel systems. (A) Inner external levee. (B) Outer external levee. (C) Internal levee or abandonment. (D) Terrace. (Modifed from Hansen et al., 2017). (E) Decay in mean thickness of sandstone within each turbidite within the external levee with increasing distance from the channel belt (redrawn from Kane et al. 2007).

Figure 10. (A) Grain-size distributions of external levee sandstones progressively further from the channel, showing only minor change in mode from proximal to distal levee. (B) ternary diagram of sand/silt/clay of external levee sandstones, showing

increase in silt away from the channel. (C) Detrital composition of sandstones and < 2cm fraction of conglomerates plotted on Dickinson (1985) provenance diagram. Total quartz (Qt), feldspar (F), and lithic (L). (D) Pie charts (by volume) of clast composition of granule/sand fraction of conglomerates, divided into stages 1 and 2 of each channel complex set, in stratigraphic order (base to the top). Colour coded by the lithologic categories. (E) Cumulative and normalized distributions of detrital zircon U-Pb ages for each channel complex set. Cumulative distributions are colored according to channel complex set. Number of samples/grains shown in parentheses. The vertical scale of normalized distributions greater than 300 Ma is displayed at 1/10th scale. Ng—Neogene, Pg—Paleogene, K—Cretaceous. The thick gray line is the cumulative distribution of detrital zircon U-Pb ages (≤200 Ma) from Peninsular Ranges batholith (PRB) from Sharman et al. (2015). The dashed red line indicates the depositional age of the San Fernando channel system.

Figure 11. (A) Differentiation of different channel-associated thin bed environments on the basis of sandstone proportion and standard deviation of bed thickness (from Hansen et al., 2017a). (B) Differentiation of different channel environments on the basis of de-trended correspondence analysis of palynofacies dataset, demonstrating spectrum groupings from channel axis through the overbank deposits. Levee categories include both internal and external levees. (From McArthur et al. 2016).

Figure 12. (A) Differentiation of different channel-related environments based on spatial distribution of key ichnofacies associations (see text). Eponymous

ichnogenera: (B, C) *Scolicia*; (D) phycospiphoniforms; (E) *Nereites*; (F) *Ophiomorpha*; (G) *Tisoa*.

Figure 13. Synthesis of evolution of the channel system through formation of one complete channel complex set, CCS-B. 1. Incision of the basal CCS bounding surface (4^{th} order surface). 2. Deposition of bypass/bedload-dominated coarse-grained material in broad, moderately aggradational, braid-like channel belt, with overspill onto terraces. 3. Development of graded (non-aggradational) meander belts, with overspill onto bordering terraces or internal levees. 4. Aggradation of channels with inherited sinuosity, with overspill onto bordering terraces or internal levees. (Multiple repetitions of 3 and 4). 5. Abandonment and drape before; 6. Re-incision at base of the succeeding channel complex set.

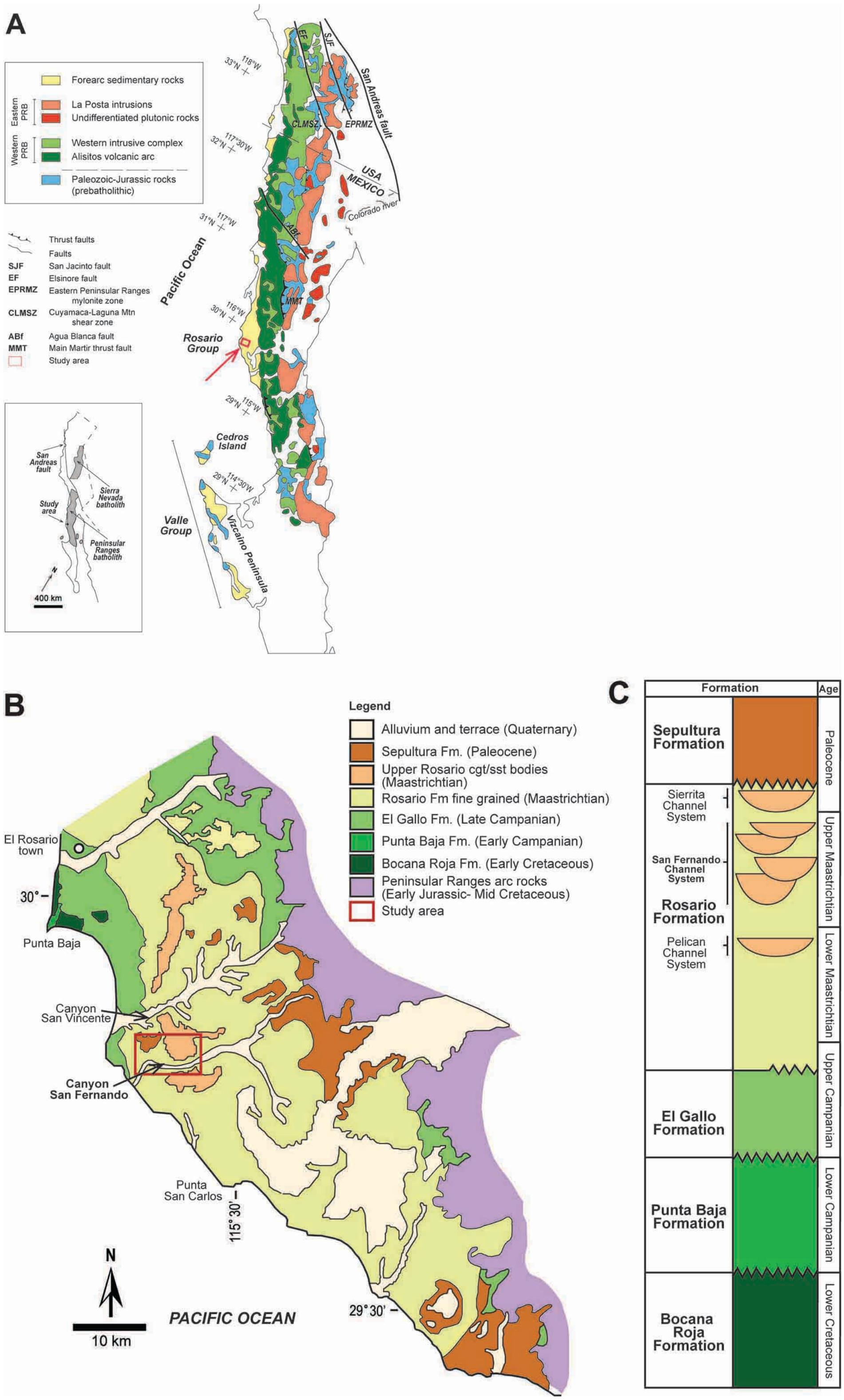
A
Forearc sedimentary rocks
Eastern PRB
La Posta intrusions
Undifferentiated plutonic rocks
Western PRB
Western intrusive complex
Alisitos volcanic arc
Paleozoic-Jurassic rocks (prebatholithic)
Thrust faults
Faults
SJF San Jacinto fault
EF Elsinore fault
EPRMZ Eastern Peninsular Ranges mylonite zone
CLMSZ Cuyamaca-Laguna Mtn shear zone
ABf Agua Blanca fault
MMT Main Martir thrust fault
Study area
San Andreas fault
USA
MEXICO
Colorado river
Pacific Ocean
Rosario Group
Cedros Island
Valle Group
Vizcaino Peninsula
33°N 118°W
32°N 117°30'W
31°N 117°W
30°N 116°W
29°N 115°W
29°N 114°30'W
San Andreas fault
Sierra Nevada batholith
Study area
Peninsular Ranges batholith
N
400 km
B
Legend
Alluvium and terrace (Quaternary)
Sepultura Fm. (Paleocene)
Upper Rosario cgt/sst bodies (Maastrichtian)
Rosario Fm fine grained (Maastrichtian)
El Gallo Fm. (Late Campanian)
Punta Baja Fm. (Early Campanian)
Bocana Roja Fm. (Early Cretaceous)
Peninsular Ranges arc rocks (Early Jurassic- Mid Cretaceous)
Study area
El Rosario town
30°
Punta Baja
Canyon San Vincente
Canyon San Fernando
Punta San Carlos
115° 30'
29° 30'
N
10 km
PACIFIC OCEAN
C
Formation
Age
Sepultura Formation
Paleocene
Sierrita Channel System
San Fernando Channel System
Rosario Formation
Pelican Channel System
Upper Maastrichtian
Lower Maastrichtian
El Gallo Formation
Upper Campanian
Punta Baja Formation
Lower Campanian
Bocana Roja Formation
Lower Cretaceous

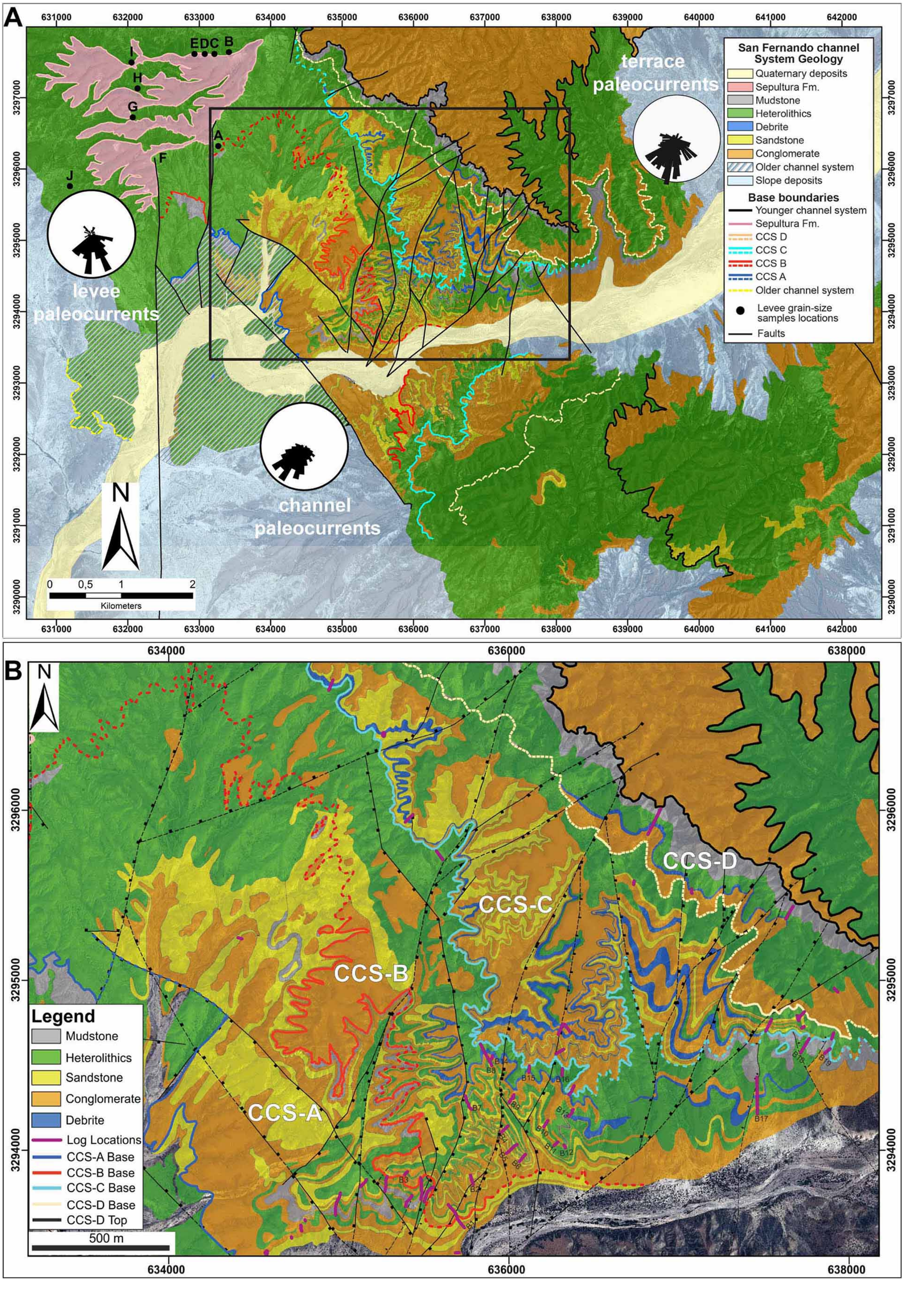
A
B
San Fernando channel System Geology
Quaternary deposits
Sepultura Fm.
Mudstone
Heterolithics
Debrite
Sandstone
Conglomerate
Older channel system
Slope deposits
Base boundaries
Younger channel system
Sepultura Fm.
CCS D
CCS C
CCS B
CCS A
Older channel system
Levee grain-size samples locations
Faults
terrace paleocurrents
levee paleocurrents
channel paleocurrents
Kilometers
Legend
Mudstone
Heterolithics
Sandstone
Conglomerate
Debrite
Log Locations
CCS-A Base
CCS-B Base
CCS-C Base
CCS-D Base
CCS-D Top
500 m
CCS-A
CCS-B
CCS-C
CCS-D

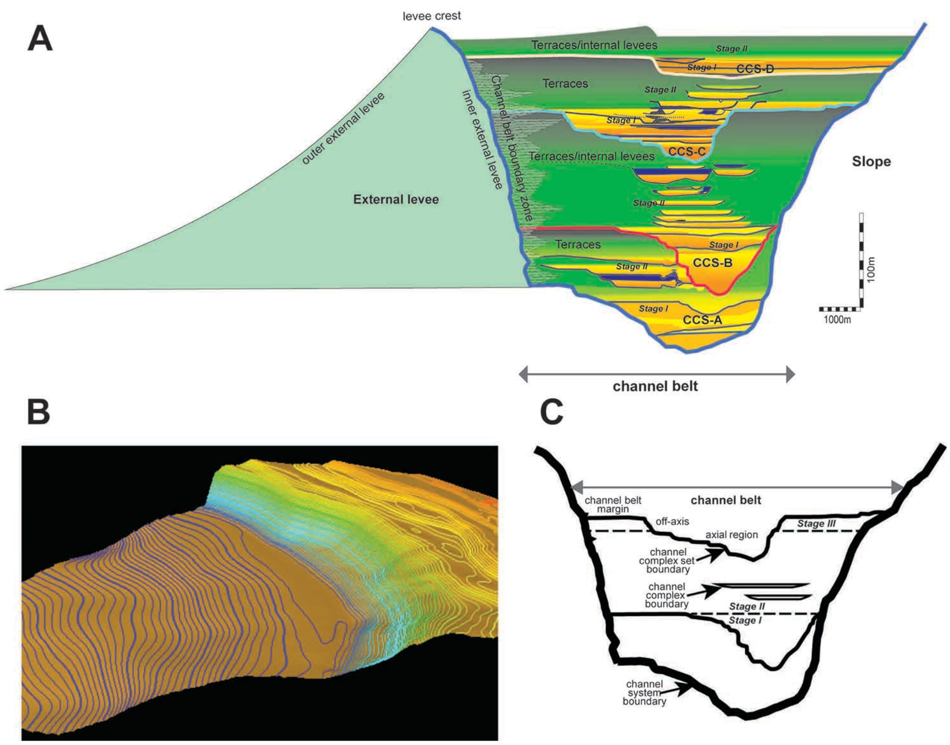
A
levee crest
Terraces/internal levees
Stage II
Stage I
CCS-D
Terraces
Stage II
Stage I
CCS-C
Terraces/internal levees
Stage II
Terraces
Stage I
CCS-B
Stage II
Stage I
CCS-A
outer external levee
inner external levee
Channel belt boundary zone
External levee
Slope
100m
1000m
channel belt
B
C
channel belt
channel belt margin
off-axis
axial region
Stage III
channel complex set boundary
channel complex boundary
Stage II
Stage I
channel system boundary

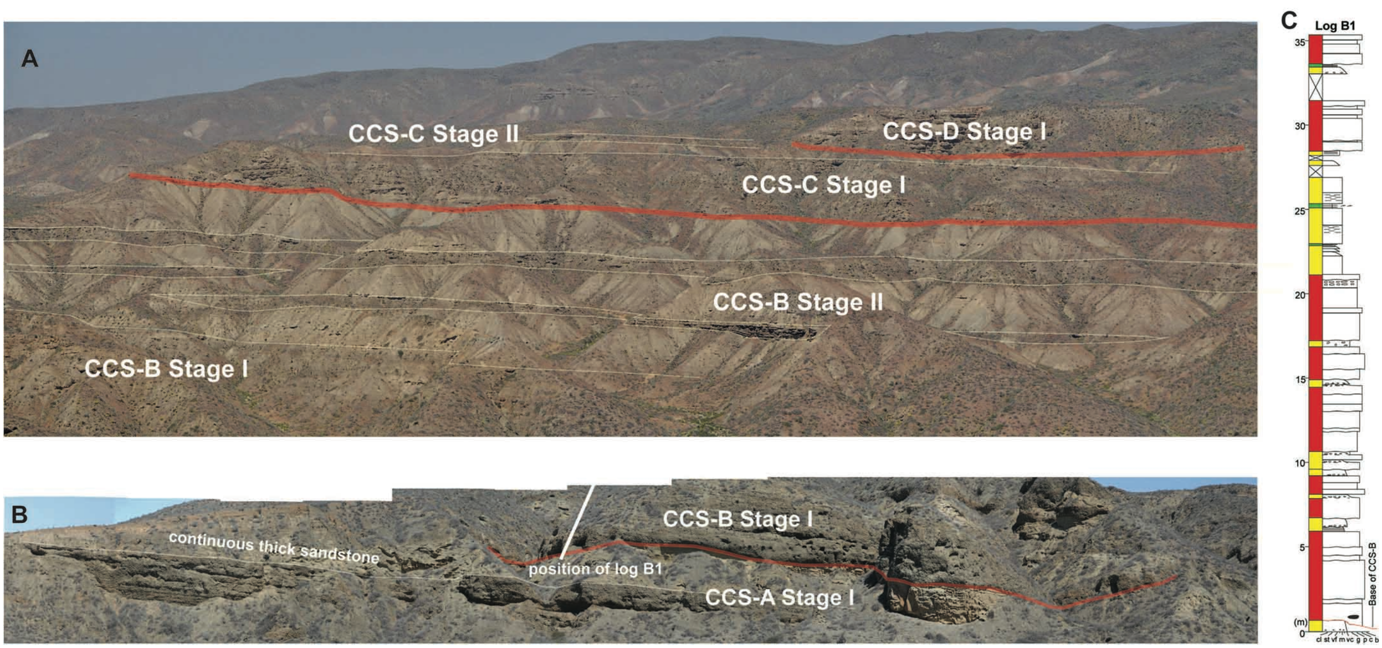

A
CCS-C Stage II
CCS-D Stage I
CCS-C Stage I
CCS-B Stage II
CCS-B Stage I
B
continuous thick sandstone
CCS-B Stage I
position of log B1
CCS-A Stage I
C
Log B1
Base of CCS-B
(m)
cl st vf m vc g p c b

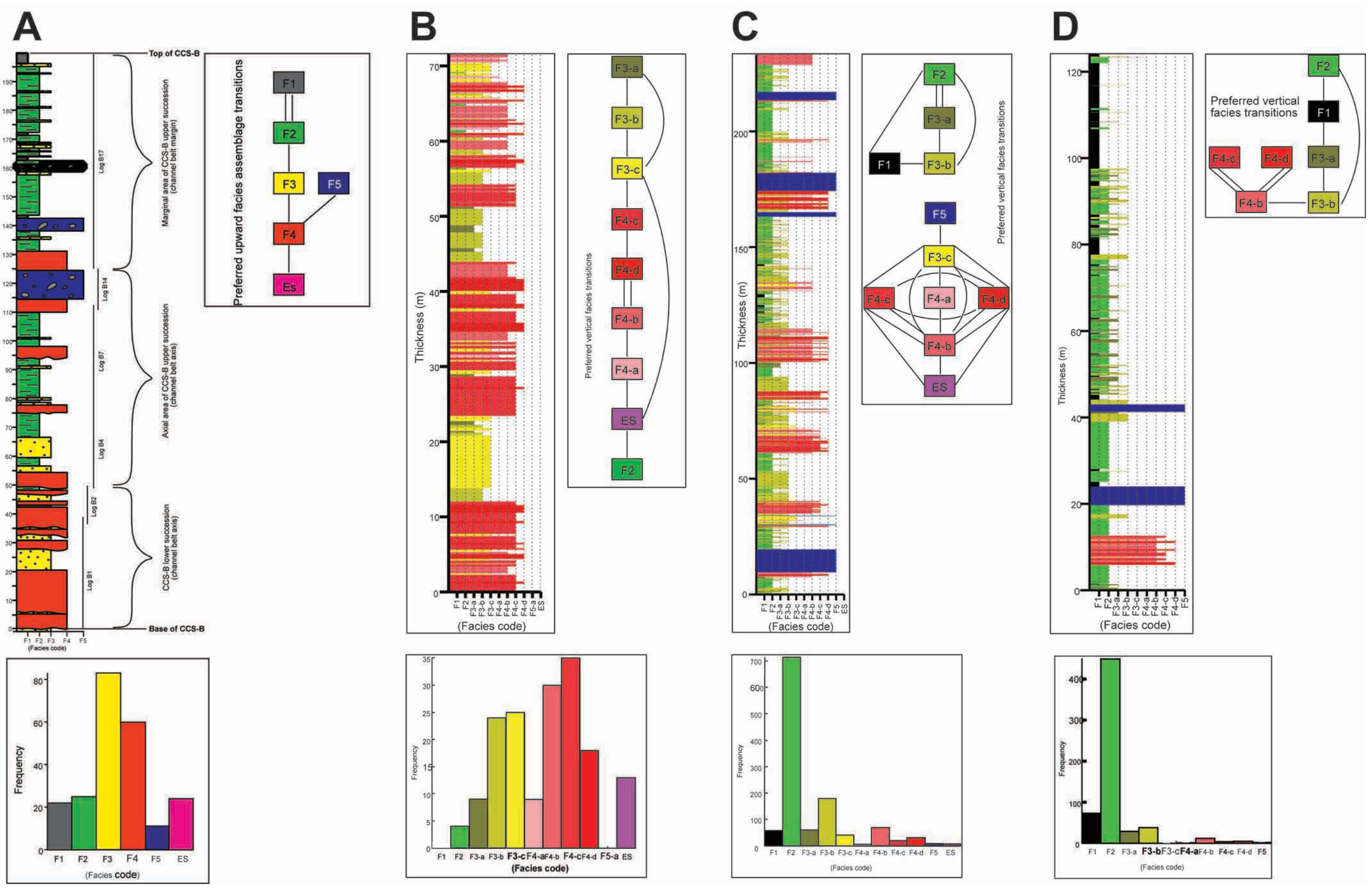
A
B
C
D
Top of CCS-B
Base of CCS-B
Thickness (m)
(Facies code)
Log B17
Log B14
Log B7
Log B4
Log B2
Log B1
Marginal area of CCS-B upper succession (channel belt margin)
Axial area of CCS-B upper succession (channel belt axis)
CCS-B lower succession (channel belt axis)
Preferred upward facies assemblage transitions
Preferred vertical facies transitions
Preferred vertical facies transitions
Preferred vertical facies transitions
Frequency
(Facies code)

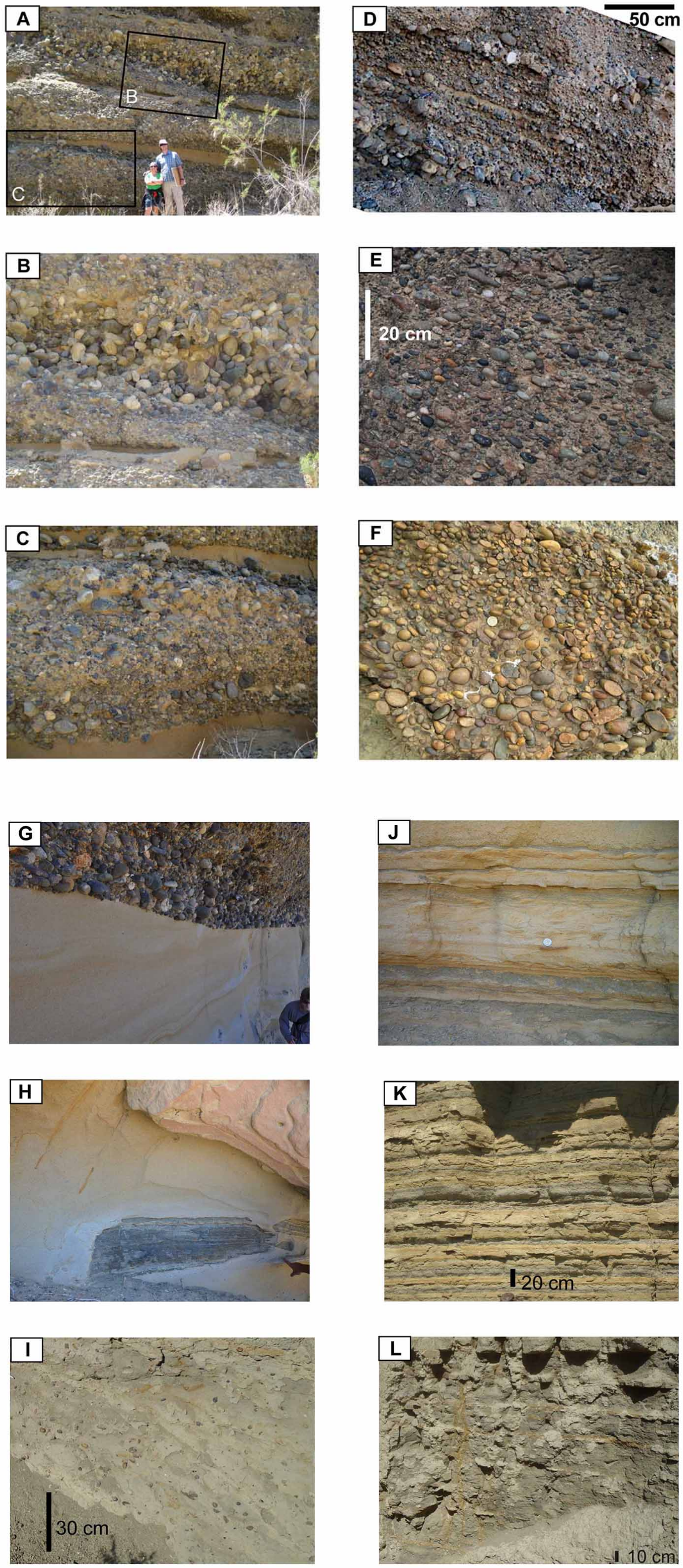
A
B
C
D
50 cm
B
E
20 cm
C
F
G
J
H
K
20 cm
I
30 cm
L
10 cm

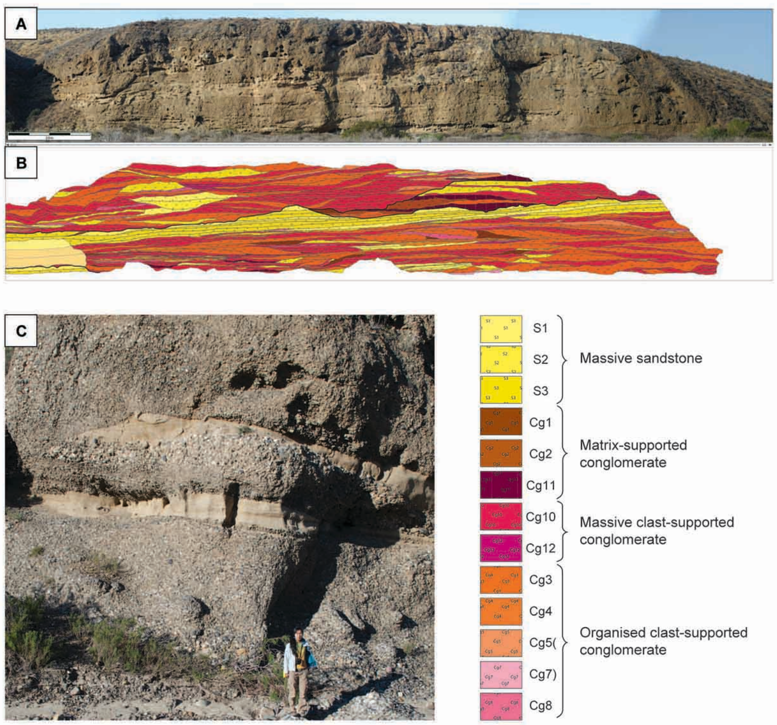
A
B
C
S1
S2
S3
Massive sandstone
Cg1
Cg2
Cg11
Matrix-supported conglomerate
Cg10
Cg12
Massive clast-supported conglomerate
Cg3
Cg4
Cg5(
Cg7)
Cg8
Organised clast-supported conglomerate

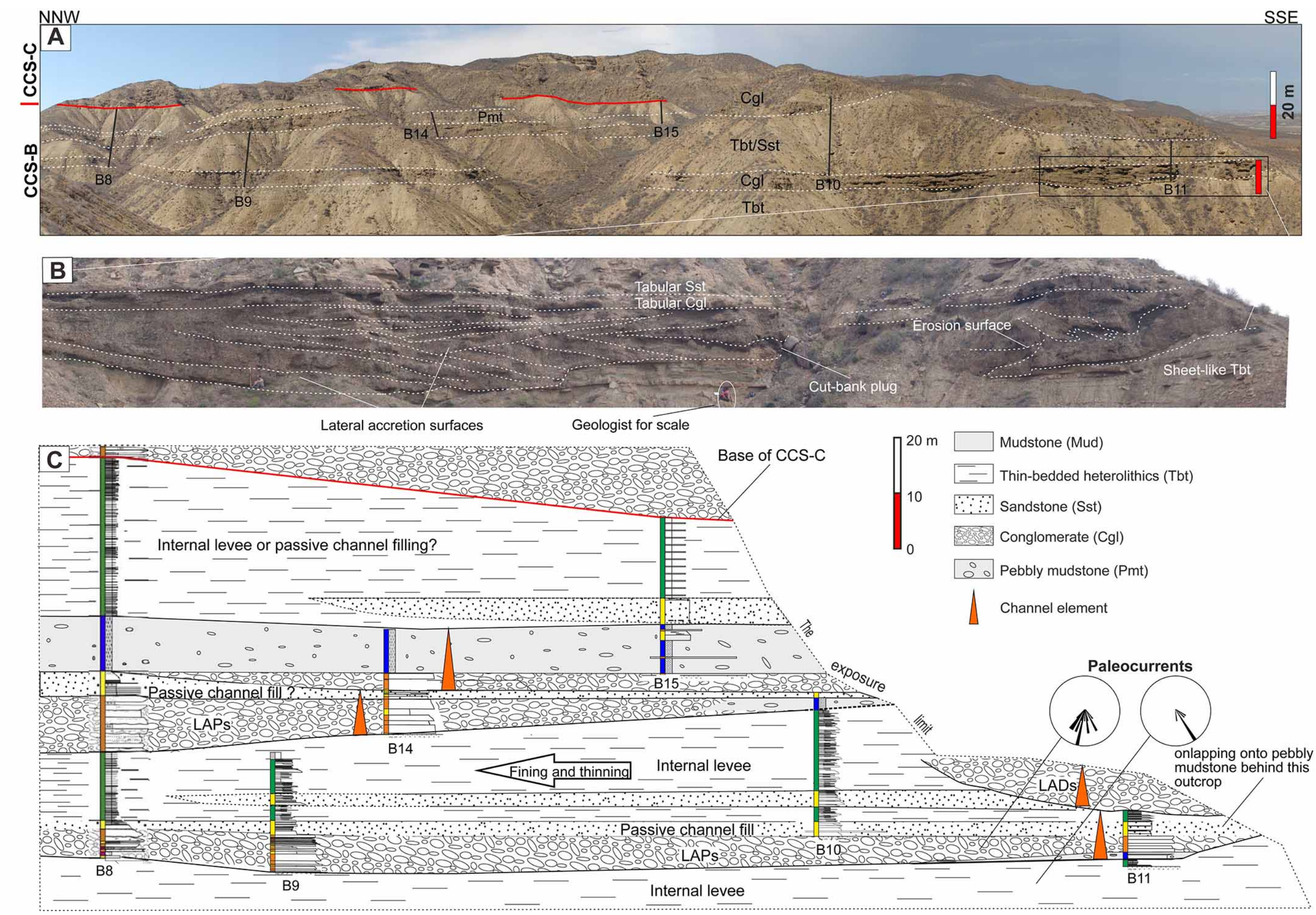

NNW
SSE
A
CCS-C
CCS-B
Cgl
Pmt
B14
B15
Tbt/Sst
B8
B9
Cgl
B10
B11
Tbt
20 m
B
Tabular Sst
Tabular Cgl
Erosion surface
Cut-bank plug
Sheet-like Tbt
Lateral accretion surfaces
Geologist for scale
C
Base of CCS-C
Internal levee or passive channel filling?
Passive channel fill ?
LAPs
B14
B15
The exposure limit
Fining and thinning
Internal levee
Passive channel fill
LAPs
LADs
B8
B9
B10
B11
Internal levee
20 m
10
0
Mudstone (Mud)
Thin-bedded heterolithics (Tbt)
Sandstone (Sst)
Conglomerate (Cgl)
Pebbly mudstone (Pmt)
Channel element
Paleocurrents
onlapping onto pebbly mudstone behind this outcrop

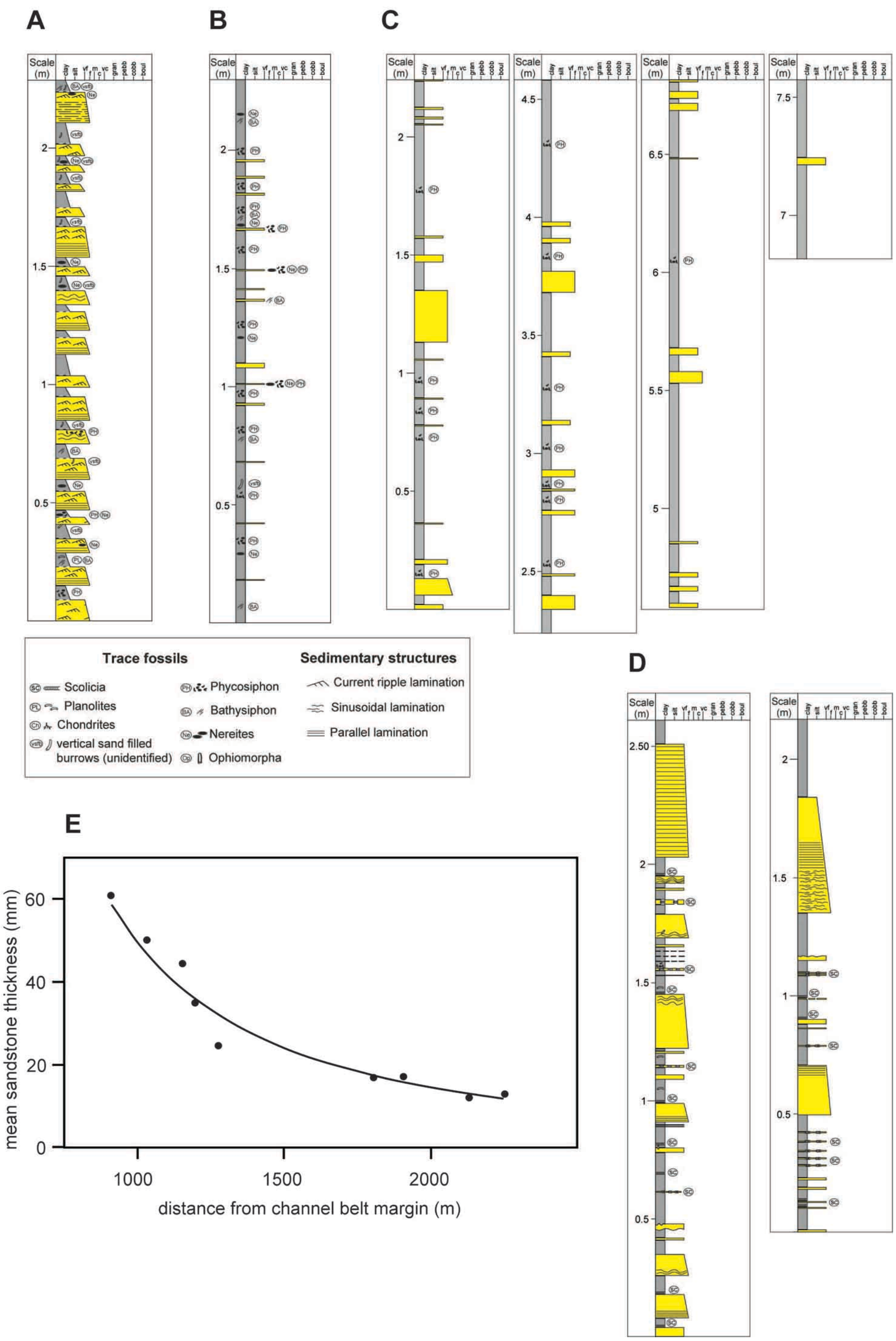

A
B
C
D
E
Trace fossils
Scolicia
Planolites
Chondrites
vertical sand filled burrows (unidentified)
Phycosiphon
Bathysiphon
Nereites
Ophiomorpha
Sedimentary structures
Current ripple lamination
Sinusoidal lamination
Parallel lamination
Scale (m)
clay
silt
vf
f
m
c
vc
gran
pebb
cobb
boul
mean sandstone thickness (mm)
distance from channel belt margin (m)

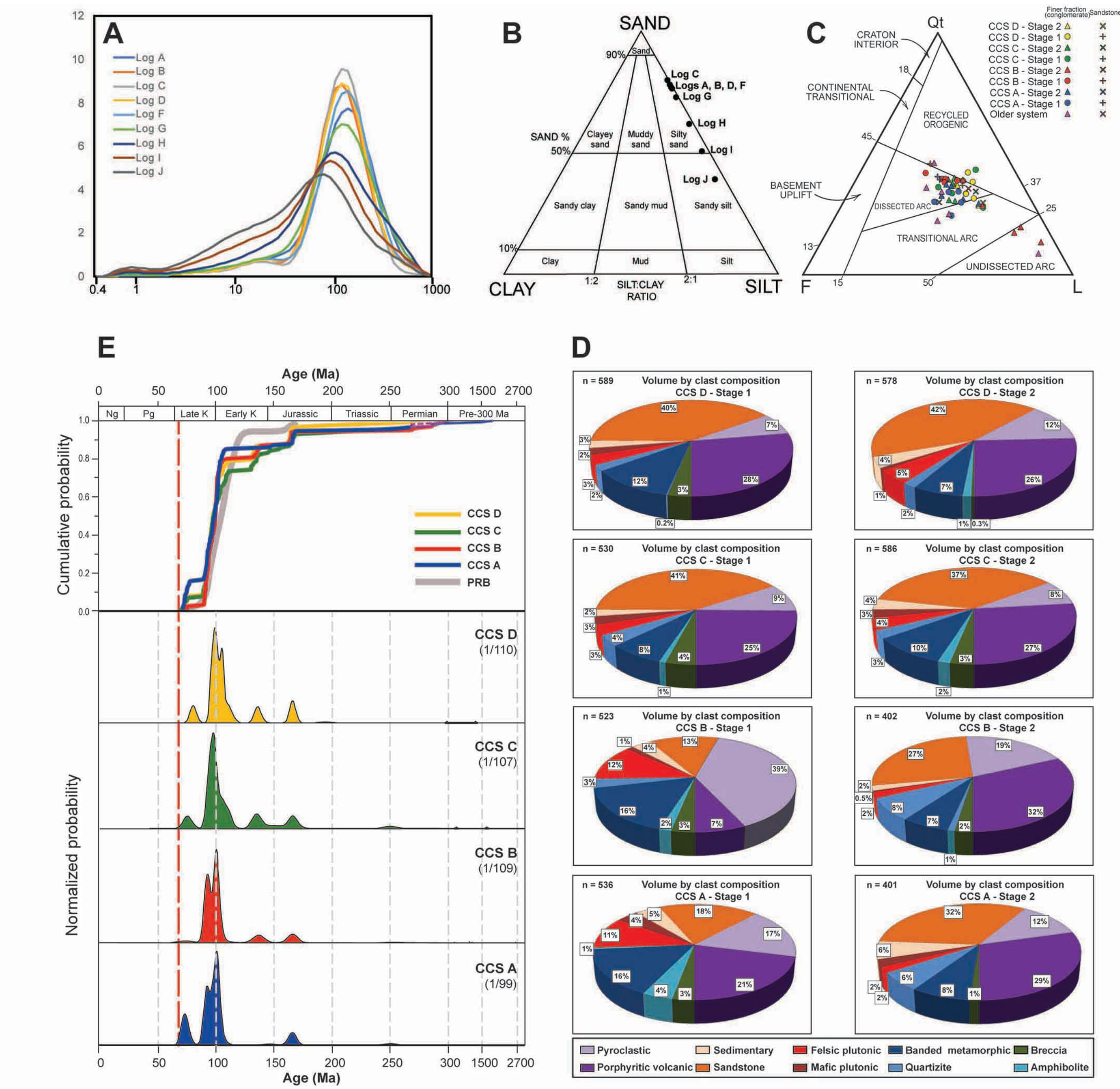

A
Log A
Log B
Log C
Log D
Log F
Log G
Log H
Log I
Log J
B
SAND
90%
Sand
Log C
Logs A, B, D, F
Log G
Log H
Log I
Log J
SAND %
50%
10%
Clayey sand
Muddy sand
Silty sand
Sandy clay
Sandy mud
Sandy silt
Clay
Mud
Silt
CLAY
SILT
1:2
2:1
SILT:CLAY RATIO
C
Qt
F
L
CRATON INTERIOR
CONTINENTAL TRANSITIONAL
RECYCLED OROGENIC
BASEMENT UPLIFT
DISSECTED ARC
TRANSITIONAL ARC
UNDISSECTED ARC
Finer fraction (conglomerate)
Sandstone
CCS D - Stage 2
CCS D - Stage 1
CCS C - Stage 2
CCS C - Stage 1
CCS B - Stage 2
CCS B - Stage 1
CCS A - Stage 2
CCS A - Stage 1
Older system
E
Age (Ma)
Ng
Pg
Late K
Early K
Jurassic
Triassic
Permian
Pre-300 Ma
Cumulative probability
CCS D
CCS C
CCS B
CCS A
PRB
Normalized probability
CCS D (1/110)
CCS C (1/107)
CCS B (1/109)
CCS A (1/99)
D
n = 589 Volume by clast composition CCS D - Stage 1
n = 578 Volume by clast composition CCS D - Stage 2
n = 530 Volume by clast composition CCS C - Stage 1
n = 586 Volume by clast composition CCS C - Stage 2
n = 523 Volume by clast composition CCS B - Stage 1
n = 402 Volume by clast composition CCS B - Stage 2
n = 536 Volume by clast composition CCS A - Stage 1
n = 401 Volume by clast composition CCS A - Stage 2
Pyroclastic
Sedimentary
Felsic plutonic
Banded metamorphic
Breccia
Porphyritic volcanic
Sandstone
Mafic plutonic
Quartzite
Amphibolite

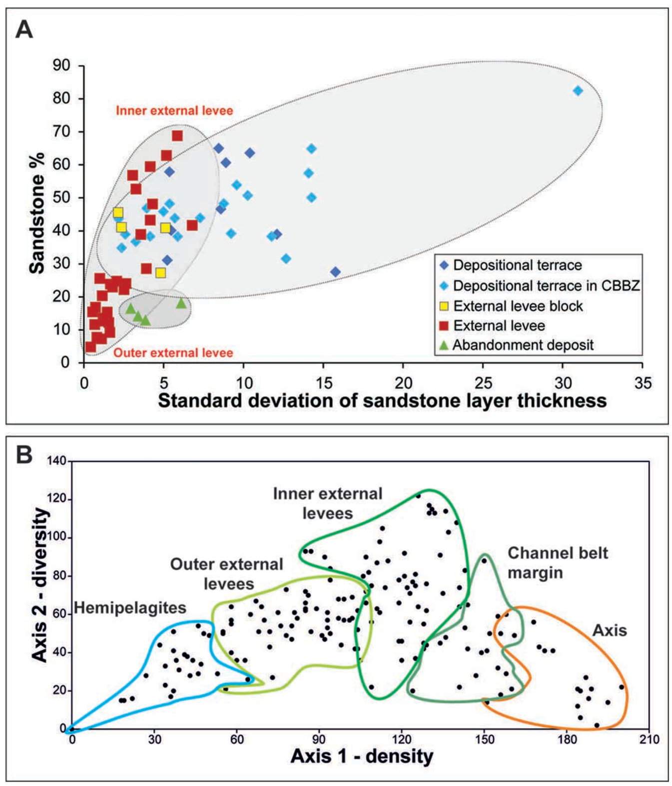
A
Inner external levee
Outer external levee
Sandstone %
Standard deviation of sandstone layer thickness
Depositional terrace
Depositional terrace in CBBZ
External levee block
External levee
Abandonment deposit
B
Inner external levees
Outer external levees
Hemipelagites
Channel belt margin
Axis
Axis 2 - diversity
Axis 1 - density

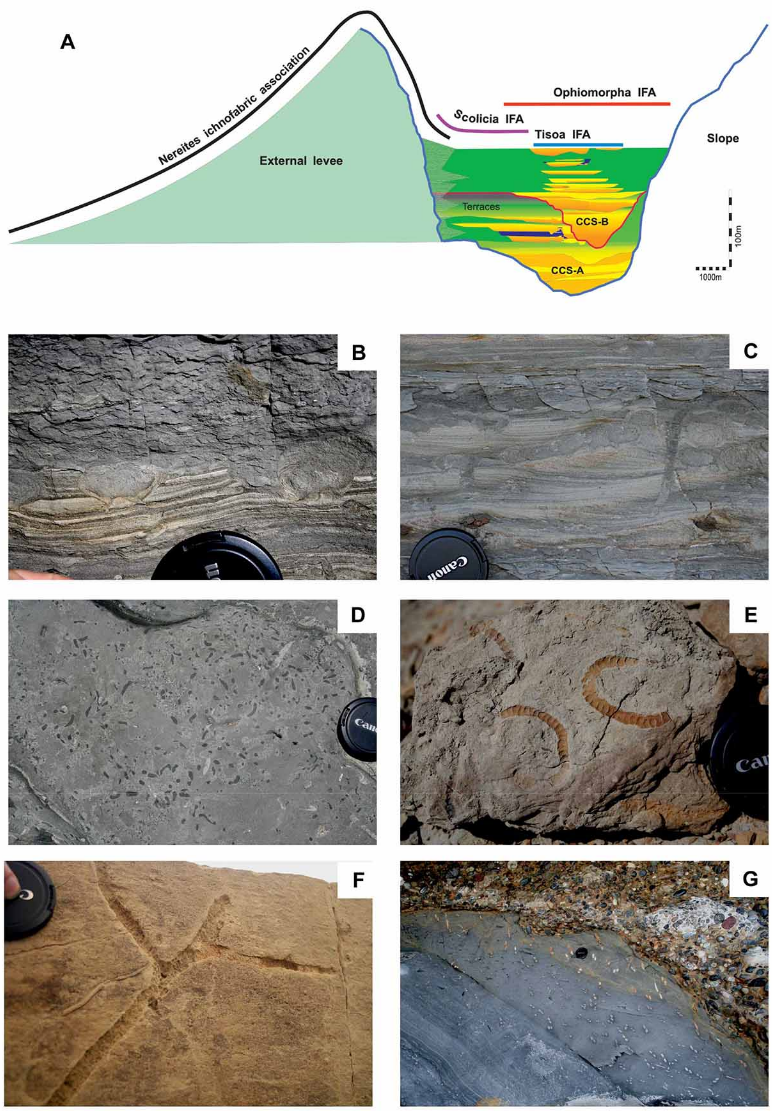
A
Nereites ichnofabric association
External levee
Scolicia IFA
Ophiomorpha IFA
Tisoa IFA
Slope
Terraces
CCS-B
CCS-A
100m
1000m
B
C
D
E
F
G

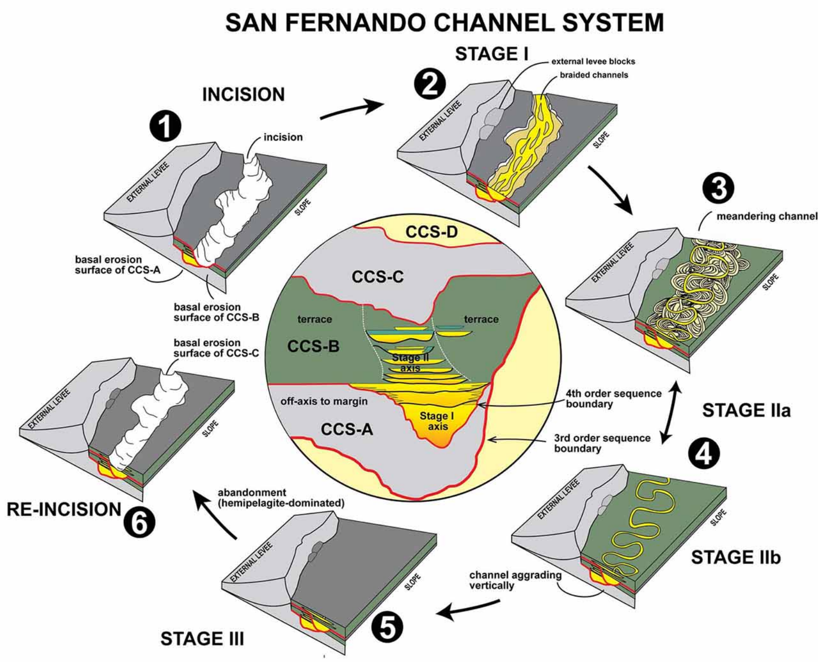
SAN FERNANDO CHANNEL SYSTEM
INCISION
1
incision
EXTERNAL LEVEE
SLOPE
basal erosion
surface of CCS-A
basal erosion
surface of CCS-B
STAGE I
2
external levee blocks
braided channels
3
meandering channels
STAGE IIa
4
STAGE IIb
channel aggrading
vertically
5
STAGE III
abandonment
(hemipelagite-dominated)
RE-INCISION
6
basal erosion
surface of CCS-C
CCS-D
CCS-C
terrace
terrace
CCS-B
Stage II
axis
off-axis to margin
Stage I
axis
CCS-A
4th order sequence
boundary
3rd order sequence
boundary